Review Article: A Comprehensive Review on Materials Having High Oxygen Reduction Reaction (ORR) Activity

Fawad Ahmad[1,*], Khusbo-e-Kainat[1], Umer Farooq[2]

[1]*Department of Chemistry, University of Wah, Quaid Avenue, Wah Cantt., (47010), Punjab, Pakistan*
[2]*Department of Physics, Division of Science and technology, University of Education, Lahore, Pakistan*

Use yor device to scan and read the article online

Citation F. Ahmad*, K.E. Kainat, U. Farooq. **A Comprehensive Review on Materials Having High Oxygen Reduction Reaction (ORR) Activity.** *J. Chem. Rev.*, **2022**, *4*(4), 374-422.

https://doi.org/10.22034/JCR.2022.357844.1185

Article info:
Received: 25 August 2022
Accepted: 5 September 2022
Available Online: 9 September 2022
ID: JCR-2208-1185
Checked for Plagiarism: Yes
Language Editor:
Dr. Fatimah Ramezani
Peer Reviewers Approved by:
Dr. Nabi ullah
Editor who Approved Publication:
Prof. Dr. Ghasem Rezanejade Bardajee

Keywords:
ORR, Electrocatalysts, Fuel cell, MOF, Oxygen reduction reaction

ABSTRACT

Several main energy conversion technologies need the improvement of extremely active, enduring, and economical catalysts for the cathodic oxygen reduction process. Some power conversion techniques including fuel cells and metal air batteries are efficient for the oxygen reduction process. The current improvements in platinum-based materials and platinum-free materials for fuel cell ORR catalysis are studied. Six primary types of contemporary ORR electrocatalysts are elaborated. Moreover, the efficiency of the resulting catalysts in respect of mass activity, kinetic current density, power density, and their inclusion into fuel cell processes, are also investigated. The benefits, drawbacks, performance of catalysts, and the need of rational design methods at the fuel-cell level are emphasized. Furthermore, the core issues, constraints, and possibilities are reviewed for developing inexpensive, more functional active, and stable electrocatalysts in the future.

List of content

***Corresponding Author: Fawad Ahmad** (fawad.ahmad@uow.edu.pk)*

1. Introduction

The atmosphere is really in great danger due to the rising global population and quickly increasing the efficient energy usage. Environment friendly and sustainable energy are more important solutions. Fuel cell technology and battery storage are commonly used for renewable energy sources [1, 2]. These are most auspicious approaches to the core combustion engines in automotive applications, and have the potential to reduce dependency on fossil fuels significantly [3]. The main fuel of a conventional polymer PEM fuel cell is hydrogen, which generates energy through water byproduct of its interaction with oxygen. ORR is used in fuel cell technology and battery storage [4]. In addition, the oxygen reduction reaction on the cathode of energy production strategies is a crucial process that lowers power transformation effectiveness [3]. The ORR becomes slow due to the huge over potential. It is a kinetically slow reaction (5 times than hydrogen oxidation process) that influences the total energy efficiency [5]. Therefore, finding electrocatalysts that can lower the ORR activated binding energy is critical for fuel cells to achieve appropriate efficiency [6]. On the one hand, ORR's kinetics demand a high concentration of valuable noble metal-containing catalysts like Platinum, which drives up the price of these electrochemical energy generation systems [7]. However, to increase the oxygen reduction process, efficient, and stable catalysts are required. Non-noble metal electrocatalysts, such as transition metal, nitrogen- carbon electrode materials, transition metal oxide, carbon materials, and MOF materials, have recently attracted the interest of researchers [5] that generalized classification is illustrated in **Figure 1**. However, because of their poor performance and stability in acidic PEMFC conditions, Pt-based catalysts retain their unrivalled advantages as an outstanding ORR catalyst. According to the report of the US Energy Department (2007) based on an estimated price of fuel cell manufacturing, the estimated cost for Pt-based catalysts accounts 56% of the fuel cell stack. As a result, the rate of platinum in the noble metal markets has a strong bearing on the price of fuel cells. Platinum's current premium pricing will almost certainly climb as demand for fuel cell energy systems grows. Therefore, the catalytic effectiveness of oxygen reduction electrode materials must be significantly modified to minimize or eliminate the need for noble Platinum [2]. Under corrosive working conditions, however, the long-term robustness of traditional ORR electrocatalysts remains a major roadblock [8]. In DOE-

monitored test fleets, fuel cell cars used $0.4mg_{Pt}/cm^2$ or more on the cathode, yet catalyst stability fell short of the industrialization goal [5, 9]. The majority of current electrocatalyst research is focused on finding ways to save money and reduce price by decreasing platinum loadings on cathode while maintaining strength and reliability. Owing to the scarcity and expensive cost of Pt, reducing its quantity and improving its catalytic activity and stability has become a hot subject. Pt_3Ni (111) had 90 times the activity of commercial platinum, which focused researchers' attention to Pt alloys [4]. The ORR activity of electrocatalysts based on both platinum and non-platinum group materials had been significantly improved. The high mass activity of 13.6 A/mg1Pt was achieved on ultra-thin sharp platinum-nanowires, when compared with commercial Platinum, which has a mass activity of 0.1-0.25 A/mg^{-1}_{Pt} at 0.9 V [1].

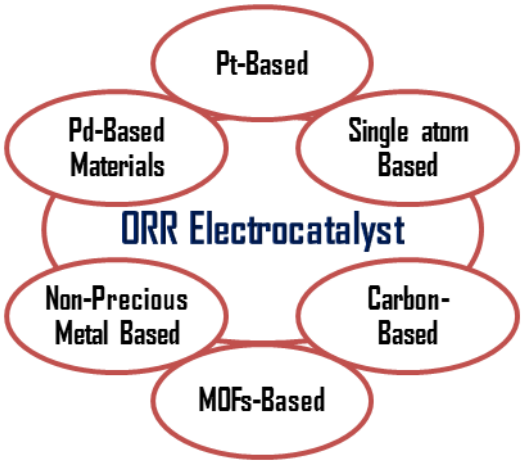

Figure 1. Different types of ORR electrocatalyst

The creation of non-noble metal catalysts is single potential technique in power conversion technologies. An extensive range of non-platinum-based materials have been developed by utilizing various synthetic techniques. The oxygen reduction reaction efficiency and durability Non-platinum of the metal catalysts were previously much under the needed limits for use in polymer electrolyte membrane fuel cells. Non-platinum-based materials includes iron and cobalt double spots implanted in nitrogen-alloyed compact carbon, outperformed commercial Pt/C in acidic environments (0.1 M $HClO_4$) [11]. Another way to decrease the Pt-loading is palladium based materials, because both have extremely comparable characteristics and are members of the same group. The oxygen reduction reaction activity of palladium is only slightly inferior to platinum, and it can be surpassed by adding an appropriate metal like cobalt or iron. In contrast, Pd's oxidation reduction reaction activity is considerably inferior than that of platinum, but it can be increased by adding a little quantity (5%) of platinum [12]. Metal-organic frameworks are a novel type of permeable material with high glass transition temperature achieved by strong interactions between metallic ions/clusters and organic ligands. MOF-based compounds have equivalent oxygen reduction reaction catalytic activities compared to commercial Platinum catalysts [13]. Heteroatoms like sulphur, phosphorous, and nitrogen doped carbons have been shown to be excellent oxygen reduction catalysts due to the interaction between the carbon and the electron density of the dopant atoms [14]. Single atom catalysts have sparked a lot of interest in the oxygen reduction process as a replacement for platinum based catalysts [1, 15].

Several studies have primarily focused on analyzing extremely effective ORR electro-catalysts that do not contain platinum or only contain trace amounts of this precious metal. In the last few decades, technology has made the significant progress in rationally designing and manufacturing superior platinum-based or platinum-free catalysts. When catalysts are reduced to nanoscale dimensions, they can

exhibit appealing physical and chemical characteristics that are not seen in the bulk state. [16]. The information about the essence of the binding sites as a result of in situ characterization methods changes conventional evidence-based testing procedures to precise formulation and construction at the subatomic and molecular levels. Enhanced electrocatalytic activity may be gained by changing the atomic structure of the catalysts, particularly the surface electronic structure [5, 17].

This review focuses on new catalysts for more economical and viable corrosive PEM fuel cells, but it is not limited to that. Non-platinum group metal electrocatalysts are often unsustainable in acid media, but they exhibit good oxygen reduction reaction potency and stability in basic medium. After detailed description of ORR electrocatalysts, which are separated into different categories including precious or noble metal materials, palladium-based materials, non-precious metal materials, MOF-based materials, carbon-based metal, metal-free materials, and single-atom based materials. The ORR activity of the six categories of electrocatalyst is also slightly addressed and compared to that of Platinum-based catalysts. We examine TMO, TMN, TMC, and chalcogenides as non-noble electrocatalyst, meanwhile certain carbon-assisted materials and single atom catalysts are non-noble metal catalysts. During the study, we explore the difficulties and prospects of alternative electrocatalysts, with a focus on practical applications, which could aid in the creation of more appealing electrode materials for fuel cells and other sustainable power solutions [1, 18].

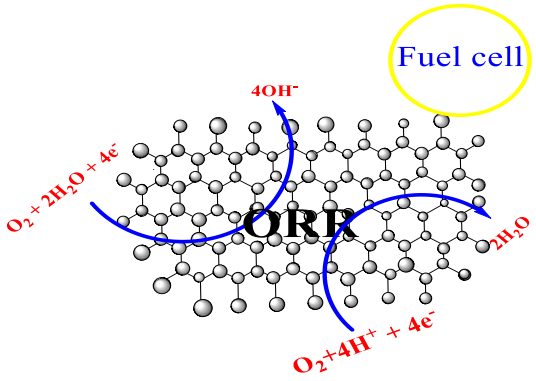

Figure 2. Reaction mechanism for oxygen reduction process in acidic and basic environment

1.1. Reaction Mechanism for Oxidation Reduction Process

Oxygen Reduction Reaction on Cathode

In Acidic Medium

Effective 4e- pathway $O_2 + 4H^+ + 4e^- \rightarrow 2H_2O$

Ineffective 2e- pathway $O_2 + 2H^+ + 2e^- \rightarrow H_2O_2$

$2H_2O + 2H^+ + 2e^- \rightarrow 2H_2O$

In Alkaline Medium

Effective 4e- pathway $O_2 + 2H_2O + 4e^- \rightarrow 4OH^-$

Ineffective 2e- pathway $O_2 + H_2O + 2e^- \rightarrow HO_2^- + OH^-$

$HO_2^- + H_2O + 2e^- \rightarrow 3OH^-$

Atomic-level description of the oxygen reduction process is still in the beginning phases due to evident intricacy of Oxygen reduction reaction dynamics. However, total four linked proton and electron transports to oxygen at the cathode are known to be required for the overall electrochemical oxygen reduction reaction, as depicted in **Figure 2** [1]. The ORR requires significantly more over-potential than the anodic hydrogen oxidation process. This is a multi-electron reaction that may contain many

elementary stages involving distinct reaction intermediates at the same time [5]. The electro reduction of O_2 can occur in different ways:

a) Reduction of 4 electrons to water in acidic environment or hydroxyl in alkaline environment,

b) 2-electron mechanism including hydrogen peroxide,

c) A ‘‘series" of passage involving two and four e- reduction,

d) A "parallel" system of channel involving processes (i) (ii), and (iii)

e) An "interactive" pathway is feasible in which species spread from series to direct channel,

f) The attachment of molecular oxygen and subsequent electron/proton transport to molecular oxygen and O_2H (reactive oxygen species), which then break down into atmospheric oxygen and hydroxyl ion, is an associative operation.

A dissociative operation is one in which the molecular oxygen is broken, as well as the hydrogenation of atomic oxygen to hydroxyl and water [5, 17].

$$1/2O_2 + * \longrightarrow O^* \xrightarrow{e^- \ H^+} HO^* \xrightarrow{e^- \ H^+} H_2O + * \quad \text{Equation 1}$$

$$O_2 + * \xrightarrow{e- \ H+} HOO^* \xrightarrow{e^- \ H^+} H_2O + O^* \xrightarrow{e^- \ H^+} HO^* \xrightarrow{e^- \ H^+} H_2O + *$$

Equation 2

$$O_2 + * \xrightarrow{e^- \ H^+} HOO^* \xrightarrow{e^- \ H^+} H_2O_2 + * \quad \text{Equation 3}$$

Where * represents the catalytically active sites.

Although the selective reduction of oxygen to hydrogen peroxide includes the undesirable 2e- route, the 4e- pathway, (step 1 and 2) is the most viable reaction mechanism for ORR (step 3). Depending on whether the chemisorbed O_2 breaks before or after protonation, stages 1 and 2 are referred to as dissociative and associative routes, respectively. The four-electron pathway should, theoretically, dominate the ORR process in the overall reduction of O_2 to water (H_2O) [19, 20]. The 2e- route, which involves incomplete oxygen reduction to H_2O_2 and is inescapable throughout the Oxygen reduction reaction, is believed to be related to a set of variables including imperfections, effective sites densities, and inter particulate spacing. However, with latest configuration, platinum-catalyst or non-precious metal catalysts, e is often minimal up to 2 percent. As a result, the following sections concentrate on the four-electron pathway [1].

The DFT simulations are frequently used to determine the free energy of intermediate compound. The principal oxygen transition products *O and *OH are implicated in both the dissociation and association pathways, with a supplemental *OOH for the others. As a result, the oxygen adsorption energy (DEO) should be investigated and used as an identifier for ORR performance. The ligand impact and the strain impact are thought to control DEO of PGM-based catalysts, whereas the locus of the d-band center compared with the Femi-level is thought to govern DEO of PGM-based catalysts. The scaling relationship among DEO and ORR has been well demonstrated in various tightly packed metal surfaces, such as "huge volcanic plots" with Pt placed throughout the optimum spot. A good target metal should have a moderate to high ability to bind oxygen. A poor contact will limit molecular oxygen adsorption and consequent breakdown to create O*, even though a strong connection will prohibit the removal of proton-coupled electron transfer intermediates (O* or OH*) [21]. Similarly "huge volcanic bends" have been created for platinum bimetallic alloys having DEO of roughly 0.2 electron volt, lower than pure platinum for the optimum model catalyst. DFT calculations are also widely used to identify patterns in catalytic activity for non-

PGM ORR catalysts. Understanding and analyzing the patterns in ORR activity on different metal or carbon-based materials requires knowledge/relationships generated by experimental studies and DFT calculations, which gives vital direction for the creation of efficient ORR electro-catalysts [1, 22].

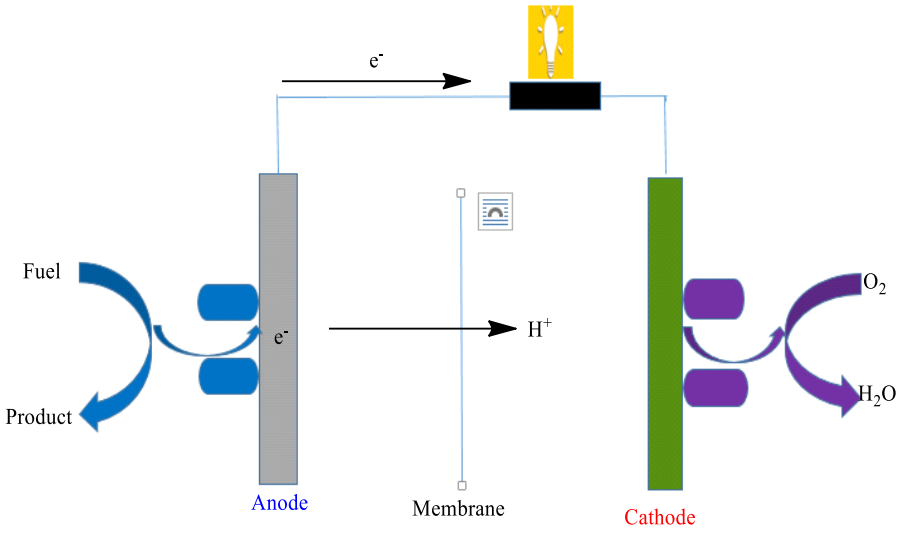

Figure 3. A schematic representation of a Fuel Cell

2. *Fuel Cell*

Fuel cells, like batteries, do not run out of energy and do not need to be recharged. As long as fuel is supplied, they generate hydroelectricity. Fuel cell is comprised of 2 electrodes that are a negatively anode and a positively cathode wrapped surrounding an electrolyte. The anode takes a fuel source, such as hydrogen or hydrogen carrier molecule, and the cathode takes oxygen called oxidant, as demonstrated in **Figure 3**. A fuel cell produces electricity by using the chemical energy of hydrogen or other fuels. Only electricity, water, and heat are produced when hydrogen is used as a fuel. Automotive, industrial, commercial, apartment blocks, and long-term grid power storage in reversible systems are the applications of fuel cell [24]. Fuel cells offer multiple benefits over conventional combustion-based technologies. Power devices can possibly be more productive than gas motors, changing the energy input into power with transformation efficiencies of up to 60%. When contrasted with ignition motors, energy units radiate less or no poisons. Since hydrogen power devices discharge water and no carbon dioxide, they can assist with settling significant environment issues. At the operative point, there are no air contaminants that cause smog or health issues [25].

Hydrogen Fuel Cells (FC) regardless of the fact that the great majority of past outstanding oxygen reduction electrocatalysts were only evaluated at the rotating disc electrode magnitude, there has recently been a significant trend toward emphasizing membrane electrode assembly testing for reported ORR electrocatalysts. The membrane electrode assembly comprises of a layer of impetus, gas dissemination layers, a proton exchange film, and exploratory investigations at the MEA level, is significantly more complicated than RDE tests. With the existing difficulties in mind, greater emphasis and effort should be placed into membrane electrode assembly magnitude and even fuel cell pile catalyst performance studies to consider and evaluate their promising applications in PEMFCs. In rotating disc electrode tests, many non-platinum based catalysts perform similarly to commercial platinum electrode materials, but in membrane electrode assembly tests, the specific density at 0.7 V and peak power density of carbon-assisted or single-atom oxygen reduction electrode material are quiet poor to Precious metal oxygen reduction catalysts. With a specific density of

1.0A/cm^2 at 0.7 volts versus reversible hydrogen electrode and an overall platinum concentration of 0.39 mg/cm^2 at both electrodes, the combination of basic platinum-cobalt nanoparticles with the cobalt doped nitrogen supported on carbon substrate resulted in highly active and stable electro-catalyst. Already, the simple solvothermal and subsequent leaching combination of grouped platinum-nickel composite nanocages was uncovered, which gave a current thickness of 1.1 A/cm^2 at 0.7 V versus RHE while diminishing the general Pt content to 0.25 mg/cm^2. A Pt-Ni nanocage power device impetus could create a current thickness of 1.5 A/cm^2 at 0.6 V versus RHE and run for no less than 8 days. Alluring MEA execution was seen on numerous SAC-based impetuses. The manufacture of a wedge molded Fe-N-C SAC with suddenly high MEA movement because of its objectively planned open mathematical structure and expanded dynamic locales was revealed. The novel catalyst's specific density was 0.047 A/cm^2 at 0.88 vs. reversible hydrogen electrode under the US Department of Energy testing procedures. In 2017, Ballard Power Grids revealed the first fuel cell system that did not use PGM-based catalysts, although the efficiency and kind of catalyst were not revealed. High-efficiency fuel cells based on non-precious metal catalysts are likely to hit market in near future, due to significant efforts from academics and industry [1].

3. *Pt-Based Materials for ORR*

The electrochemical process in cathodic ORR wants to be accelerated to acquire desired output due to its sluggish kinetics. So far, among all the catalyst available for ORR, platinum based electrode materials are the best one for its outstanding performance toward ORR (**Figure 4**). Due to this unique property, Pt-based catalyst are irreplaceable [26]. Beside the best performance of ORR, the major obstacle is the Pt price that is rising abruptly and rapidly and insufficiency of Pt. That's why platinum is considered as industrial metal over precious metals [17]. According to an estimate by the US Energy department (DOE), the sky rocketing price of platinum bestow to about 41% of the total price of fuel cell stack. DOE has set a distinct goal to lower the amount of platinum to 0.125mg$_{pt}$/cm^2 for fuel cell. ORR is enough delicate to the surface electronic properties [26].

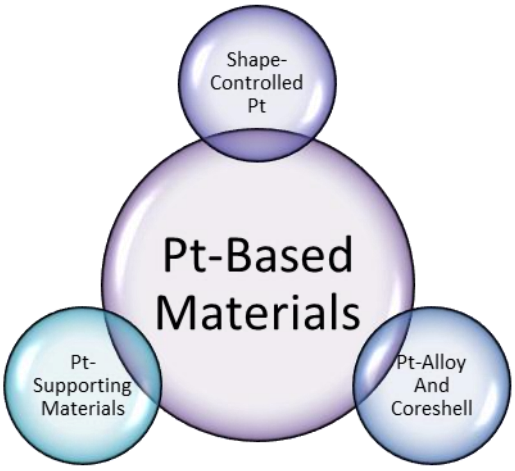

Figure 4. Pt-based materials for ORR

The efficiency and durability of Pt-based catalysts can be boosted by manipulating surface electronic properties. This process also increases the catalytic activity. The surface electronic properties can be controlled in four different ways: (i) Manipulating the visible facets of platinum and this result in maximum activity of platinum towards ORR, (ii) Fusing the platinum with the other metals to obtain multi-metallic alloys because bimetallic system shows high performance, stability, and durability as compared with single atoms, (iii) Introducing some foreign species by modifying the platinum catalyst surface such as organic compound and

metal clusters, and (iv) Selecting such a catalyst which has high corrosion resistance. In this section, the recent advancement in platinum-based catalyst will be reviewed [6, 8, 17, 27, 28].

4. *Shape-Controlled Catalyst*

Platinum-based materials show 2 to 3 time's higher activity than platinum. To enhance the system activity and performance of the fuel cell, the platinum loading should be reduced. When particles are reduced to nanoscale size, most of the physiochemical properties that aren't visible in the bulk form become visible, expanding the possibilities for making less price platinum based materials for fuel cell tenders. Shape-controlled platinum derived catalysts have ten times the mass activity and current density, as compared with commercially available platinum catalysts [27]. Shape controlled Pt-based catalyst are classified into polyhedra, Pt-nanocubes, Pt-nanoframes, and Pt- based nanowires.

Sides and border regions usually assist to the catalysts performance in nanomaterials with diameters less than 5nm. The ORR current density increases by a factor of four when the grain size is altered from 1.3 to 2.2 nanometers. The oxygen energy gap of platinum spots on cuboctahedral granules is assumed to be linked to these particle diameter-dependent properties. Because the fraction of border and corner spots drops as nanocrystals grow larger, there may be an "exchange" among both surface area and current density, resulting in a dimension-dependent peak value of overall efficiency for such electrocatalyst [16, 29].

Pt_3Ni nanoctahedra was prepared by the reaction of platinum acetate, nickel acetate, oleylamine, and oleic acid in three neck flask under an organ stream in the presence of $W(CO)_5$. Later on, it was revealed that $W(CO)_5$ was responsible for Pt_3Ni shape control. The Pt_3Ni nanoctahedra yield was approximately 80%. Pt_3Ni nanoctahedra were found to be stable and had an exterior surface separation outline compared with that of elongated Pt_3Ni surfaces, according to Monte Carlo simulations. As a result, numerous researchers have reported high ORR activity after forming octahedral Pt_3Ni particles, demonstrating that the strategic approach is able to solve catalyst problems [30]. Pt_3Ni single crystal surfaces have a continuous rise in ORR activity over Pt and a 90-fold rise over the present condition of Pt/C catalysts. The prepared nanoctahedra Pt_3Ni shows a boundless ORR mass activity of $2.67 Amg_{pt}^{-1}$. Glucosamine was used as a reductant, and chloroplatinic acid and nickel chloride were liquefied in deionized water with forcefully stirring in an airtight, PTFE-lined vessel to make Pt_3Ni icosahedra nanocrystals. After 30 minutes the precursor solution was added in an autoclave at 180 °C for 6 hours. Later on, separation was done by centrifugation and scrubbing with deionized H_2O, ethanol, and Pt_3Ni icosahedra nano electrocatalyst was acquired. When contrasted to conventional platinum catalyst, Pt_3Ni icosahedra nanostructures have 32 and 12 times boost in current and mass activities, correspondingly. Pt_3Ni icosahedra nanocrystals, for example, have one of the highest ORR mass activity value is$1.761\ A/mg_1$ Pt and current density value is $6.38 mA/cm^2$ Pt yet reported for energy storage applications [29].

Platinum acetate ($Pt(acac)_2$), oleylamine, and oleic acid were used to make Pt_3Ni nanocubes in a three-neck flask under an argon stream. Tungstun hexacabonyl $W(CO)_6$ was introduced into the strenuously stirred solution. After that, a Ni-precursor standard solutions was made by dissolving $NiCl_2{\cdot}6H_2O$ in a mixture of solvents comprising oleylamine and oleic acid. The temperature was gradually increased from 130 to 240 °C and stock solution was added drop wise. The yield of Pt_3Ni nanocubes was approximated to be around 70%. Without $W(CO)_6$ Pt_3Ni nanocubes can also be prepared but their shape is less controlled. It is clear that the ORR activity is reliant on the particle shape and the composition. As prepared Pt_3Ni nanocubes shows a mass activity of $0.62\ Amg_{pt}^{-1}$. The same procedure used to make Pt_3Ni nanocubes was used to make platinum nanocubes, except for the Ni precursor absence [26]. Because of their reasonably large effective surface area platinum atom consumption, Pt-based nanoframes have emerged as among the most efficient and long-lasting ORR catalysts in the last two years. Pt-based nanoframes were

created by folding two atomic layers of platinum into 3D Pt_3Ni nanoframes, which exhibited unexpectedly high activity, stability, and reliability during the redox reaction. Pt_3Ni nanoframe catalysts have a unique design that allows for a better utilization of platinum atoms on the surface due to their open 3D porous structure (**Figure 5**). It is widely recognized that pt-based nanoframes catalysts have a higher durability and stability due to their highly uniform crystal surfaces because nonfunctional sites on the nanoparticle surface are simpler to dissolve. Furthermore, because of the standardized homogeneous composition, big particles become bigger and fine particle shrink in size, reducing the Ostwald ripening procedure. Therefore, the Pt-based nanoframe is one of the most favorable, durable, and highly stable catalysts. The 3D Pt-based nanoframes imparted a diverse number of effective spots on both the interior and external surfaces, making the oxygen reduction process easier and boosting the electrocatalyst's overall effectiveness. The precise development of the frame structure and morphology in Pt-based nanoframe catalysts is a significant challenge. The slightly elevated facet has recently been discovered to be responsible for such outstanding results [31].

Nanowires and nanotubes are 1-dimensional nanostructures based on Platinum monocrystal nanostructures that develop along a definite path of a lattice nucleus. These Pt-based nanostructures can reduce the inserted points at the electrode-catalyst interface, allowing the catalyst to perform at its full potential. For the time being, a smaller number of particle junctions can improve electron transmission. Because of the excellent electronic transmission and dispersion of Platinum nanoparticles, 1D Pt-based nanowires and nanotubes have shown a better ORR activity. Nanowires and nanotubes with high-index substrates were created to improve ORR activity. Huang *et al.* created a unique 3-dimensional strand of Pt–Co nanowires with well-proportioned high-index aspects. This research revealed the most practical and efficient method for maximizing platinum atom consumption in poly-metallic nanowires with large surface areas. Huang *et al.* also revealed that the mass activity of prepared Pt_3Ni Nanowires was 3.96 A/mg_{Pt}^{-1}. Pt-based nanowires and nanotubes can be incredibly reliable, with almost no noticeable loss after multiple potential periods in RDE. The stability and durability of Pt-based 1D nanowires and nanotubes have been demonstrated, but high index facets on the surface of nanoparticles cause instability and make control difficult. If the facets of Pt-based NWs and NTs change, the ORR activity decreases [4].

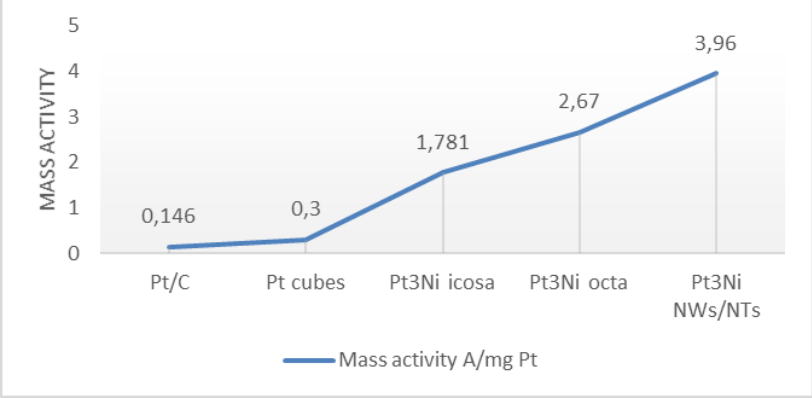

Figure 5. Mass activity of different Pt-based shape controlled catalyst

5. Pt-Based Alloys

Platinum has been reported to be alloyed with various elements, including vanadium, chromium, titanium, manganese, iron, cobalt, nickel, tungsten, molybdenum, iridium, palladium, and zinc. Using potentio dynamic RRDE measurements, a rise in ORR activity of alloy catalyst was observed as compared with the pure Pt of 1.5 to 5 times. It was also

discovered that the ORR on a Pt alloy catalyst has a 20-40 millivolts lower over potential than solo Pt [32]. Platinum group metal alloys have been attaining the maximum electrochemical stability, as compared with Platinum. The Pt_3Ni exterior is preferred for its strong mass action against ORR. The fraction of accessible platinum exterior employing cuboids and other prismatic crystals was found to boost oxidation reduction catalytic efficiency and durability for Pt_3Ni nanocrystals. The measured ORR activity enhancement in Pt alloy electrocatalyst is mostly due to a change in platinum's interface electronic characteristics, which results in higher in Oxygen reduction performance in Platinum alloy electrocatalyst [9].

Poly-crystalline hybrid layers of platinum and metals catalysts (metal may be nickel, cobalt, iron, and titanium) were made to investigate the influence of 3d metals on the catalytic ORR efficiency of Platinum alloys. It was observed that the strong ORR efficiency of these platinum blends is attributable to 3d transition metals. The d band center and the catalytic performance of platinum blends are demonstrated to have a key relation. The optimum catalytic efficiency was directed by an equilibrium between absorption coefficient of energies of reactive species and the outer layer covered by spectator species, which resembled a volcano [32]. The Pt-alloys, which are the best Oxygen reduction electrocatalysts, attach oxygen molecules weaker than pure platinum and have the highest ORR activity. The most appropriate alloying elements are nickel, cobalt, and iron. In both ORR current density and mass activity, the volcano type behavior of electro catalytic activity was exposed, which was dependent on the type of 3d metal ion. Bimetallic Platinum based electrode material for ORR has formerly been thoroughly explored [17, 31, 33]. Bimetallic platinum-cobalt Pt_3Co is one of the most potent bimetallic catalysts (**Figure 6**). After witnessing the highest ORR catalytic efficiency and stability of a bimetallic catalyst, we hypothesized that by introducing gold or iridium to a Platinum 3d bimetallic system could affect the oxygen reduction catalytic performance. We achieved adjustment knob of the oxygen reduction reaction electrocatalytic efficiency towards the volcanic apex after inserting gold, suggesting that the ternary catalyst platinum-gold-cobalt blends exterior binds oxygen weakly than platinum but somewhat higher than platinum-cobalt. The ternary composite catalyst Pt-Au-Co has a current density of 1.41 $mA.cm^{-2}$ at 0.9 Volts, which is much higher than the binary alloy catalyst Pt_3Co. Substituting Iron for the binary alloy catalyst, platinum-cobalt does not result in desirable Oxygen reduction electrocatalytic efficiency. Following 100,000 potential loops, Pt-Au-Co shows a 25% drop in the current density, while binary alloy catalysts show an 80% loss in specific activity. After 100,000 loops, the current density of Pt–Au–Co is 140 percent higher than that of platinum-cobalt [34].

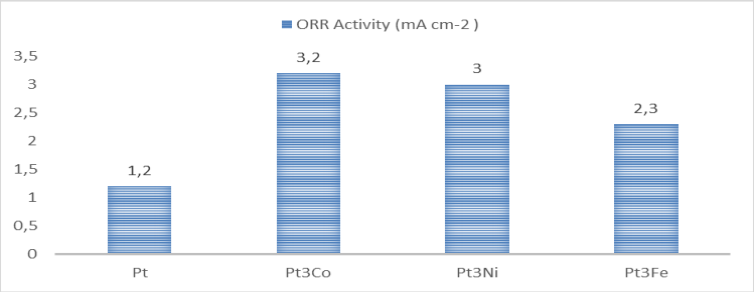

Figure 6. ORR activity of Pt-based multimetallic catalyst

6. *Surface Modified Pt-Based Materials*

Aside from regulating the exterior faces of platinum nanomaterials and combining platinum with certain additional metals to create binary alloy nanostructures, ternary nanostructures in the form of composites, and core–shells strands. Platinum electronic properties can be improved by adding metals complexes, molecular species, carbonaceous,

and inorganic component to the outer surface of platinum nanocrystals, which is beneficial to the ORR activity. The ORR catalytic performance was improved in surface modified Pt-based materials, which was dependent on covalent and non-covalent interactions on the platinum electro-active facets for ORR. In an intense adsorptive H_2SO_4 solution, molecular sorption of melamine over Pt[111] surface resulting [Pt{111}–Mad], the Oxygen reduction efficiency can be increased massively when matched to bare Pt[111]. Although the ORR is unobstructed, the sorption of melamine on the platinum surface specifically obstructs the sorption of bisulfate ions, resulting in the toxicity of the Pt[111] surface. Compared with cyanide species adsorbed on the Pt[111] exterior, the melamine-based Pt-surface 111 has better chemical stability. In a H_2SO_4 environment, Pt[III]-Melaminead has a nine fold higher ORR efficiency than pure Pt[III]. The greater consistency of the Pt[111]–Melaminead edges is attributed to melamine capacity to establish intermolecular hydrogen bonds, which effectively transform melamine components into bigger supramolecular bodies with countless attaching spots, making them more difficult to remove [35].

Carbon assisted platinum and platinum-metal (Metal: iron, cobalt, and chromium) hybrid catalysts are made by using the poylol reduction technique. In this method, metal components were simultaneously reduced and broken down with 1, 2-dihydroxyhexadecane in the presence of Pelargonic and nonylamine safeguarding reagents. According to Xiaong *et al*., who used a reduced-temperature reduction procedure with HCOONa to synthesize multiple carbon-assisted platinum-metals electrocatalysts, the platinum-cobalt electrocatalyst had the best results, with the highest catalytic properties and the least polarity when compared with traditional Platinum catalyst (**Figure 7**). The catalytic ORR activity of platinum bimetallic alloys containing cobalt, iron, and nickel created by vapor deposition was examined, with highest activity found at 40, 50, and 30%, respectively. The maximum increase in dynamic flux density was 20 times that of bare platinum. At both low and high current densities, carbon-assisted platinum-metal (cobalt, iron, and chromium) catalyst produced by the poylol reduction process outperformed conventional platinum catalysts with moderate polarization losses. In addition, the constant current voltage of carbon-assisted platinum-Iron, platinum-cobalt, and platinum-chromium electrocatalysts is 0.53, 0.59, and 0.61 Volts, respectively, which is higher than that of as-prepared and traditional platinum catalysts. The power density rises as the cathode material is detected, from platinum 7 to 10 mW/cm^2 to platinum-metals alloys, which were 16, 20, and 21 mW/cm^2 for platinum-iron, platinum-cobalt, and platinum-chromium electrocatalysts respectively (**Figure 8**), and this improvement would be due to alloying effect and supported on the carbon surface. Pt alloys had 1.5 times the ORR and a lesser voltage across a potential of 50 mV than commercial Pt/C catalysts, according to electrical and chemical studies [32].

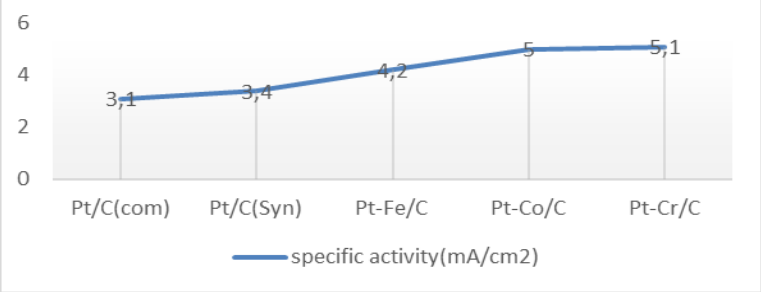

Figure 7. Specific activity of Pt-supported materials

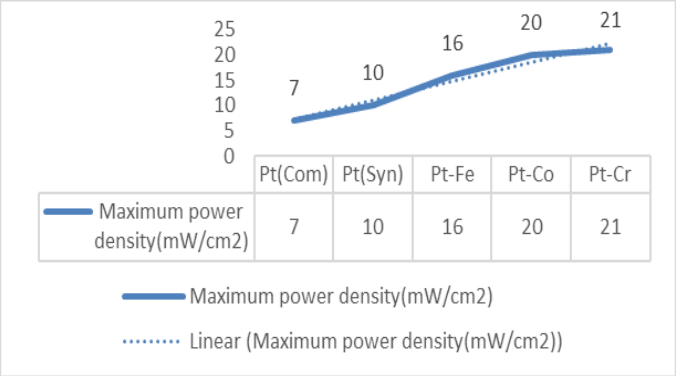

Figure 8. Power density showed by different Pt-supported ORR catalyst

7. *Pt-Free Catalysts*

The slow kinetics of the ORR and the increasing costs of platinum catalysts, are stifling the quick growth of fuel cells. Therefore, it is quite interesting to avoid Pt-based catalyst and explore the new advanced and cheaper non-platinum electrocatalyst for ORR process in fuel cells that will result in improved ORR activity. Many studies have been published to cut the price of Pt by lowering Pt amount by tuning the electronic surface of platinum, which is used to make binary and ternary alloys, introducing foreign species, and manipulating Pt's exposed faces. Further Pt-free catalytic materials lead to the significant cost reductions. In this section, our emphasis is on development of Pt-free less expensive materials that are accountable for achieving the maximum oxygen reduction efficiency and material stability that is closed to the Pt catalyst. Pt-free less expensive materials includes the cheaper Noble metals (Pd, Ir, Ru, and Ag), cheaper non-noble metals(Cu), non-precious metal catalyst (M-N-C, $MO_{x,}$ MN_X, and MC), metal organic frameworks based materials, and carbon-based materials [5, 17, 18].

8. *Palladium-Based Catalyst*

Alternative options to platinum include palladium, iridium, ruthenium, gold, and silver derived catalysts. Palladium and silver have received much interest in comparison to those other heterogeneous catalyst because of their greater oxygen reduction activity, reliability, enormous amount, and low price. Due to much less cost of Pd., fuel cell manufacturer switched from Pt-based catalysts to palladium based catalyst. Palladium and platinum belongs to same group in and have comparable properties. Pd shows very close activity to ORR and exhibit lesser over potential for ORR [17]. It is possible to improve the catalytic efficiency of Pd-catalysts by altering their electronic properties [5]. Adding exotic species to palladium is one way to change the electrical properties of the metal. Several palladium metals (iron and cobalt) bimetallic are being cast-off as oxygen reduction catalysts in recent years to improve Pd's ORR electrocatalytic performance and stability. It has been proposed that the active metals in Pd-M alloys operate as a place for O_2 bond splitting, resulting in adsorbed oxygen that transfers to porous areas guided with Palladium. There are many structures like Cu-Pd, Mo-Pd, and Co-Pd are similar in activity to Pt in catalyzing the ORR [12].

Bimetallic alloy Pd-cobalt was examined for Oxygen reduction efficiency with a diversity of palladium and cobalt atomic proportions, and resulted in the maximum catalytic performance equivalent to Platinum. It was also discovered that as the degree of alloying increases in Pd: Co with a molar ratio of 70: 30, the ORR performance decreases. Contrarily, the maximum ORR activity was achieved in Pd-Co catalysts due to the maximum Co content in alloy and minimum Pd-Pd interatomic distance. Due to presence of the maximum amount of Co, particle size of metal decreases and surface area of prepared catalyst increases. This results in maximum stability and durability of Co-Pd catalyst. The specimen treated at 350 °C demonstrated a good balance of maximum

catalytic stability and efficiency for ORR at cathode. The ORR performance of a ternary Pd-Co supported electrocatalyst was also investigated. Gold (Au) was added to binary Pd-Co electrocatalyst. The ORR performance of the ternary prepared Pd-Co-Au electrocatalyst is higher than that of the commercially prepared platinum catalyst. Another ternary Pd-based catalyst was created by mixing Mo into Pd-Co motivator. The result was ternary Pd-Co-Mo, which had better ORR catalytic activity than commercial platinum catalyst and stable performance than previously prepared Pd-Co-Au (**Table 1**) [12, 36].

Another Pd-Fe catalyst was studied with different Fe ratios. The oxygen reduction efficiency of prepared several bimetallic palladium-iron was studied. Compared with conventional platinum, this resultant bimetallic Pd-Fe with atomic ratio of 3% had the highest oxidation reaction efficiency and improved catalytic stability. Other binary catalysts of Pd was studied extensively in acidic medium like Pd-Cu, Pd-Cr, Pd-Ni, Pd-S, and Pd-W. Except for Pd-S, all of these catalysts have the highest ORR catalytic performance in contrast to platinum and nearly equivalent stability to pure palladium [37].

Table 1. Activity of different Pd-based catalyst in different medium

Reaction	Catalyst	Activity
ORR	Pd, Pd-M (M: W, Ni, Mo, P, Cu, Fe, Au, Se, Co, Cr), and Pd-Co-M (M: Mo, Au)	Pd-Co-M > Pd-M ≥ Pt > Pd
Methanol oxidation reaction	Pd-M (M: Fe,Au,Co), and Pd	Pt ‹ Pt-M,Pd
Ethanol oxidation reaction	$Pd_{85}Co_{15}$, Pd	$Pd_{85}Co_{15}$ > Pd > Pt

Facet engineering resulted in the creation of Pd-supported ORR catalysts, which will greatly improve ORR activity and durability. The ORR performance on Pd single crystals has been monitored in the past, and the results show a pattern opposite than that of platinum, namely Pd(100) ‹ Pd(111) ‹ Pd(110), suggesting that the Oxygen reduction surface region on the Pd (100) side is perhaps the most effective. The catalyst particle size and superficial strain should be controlled through manipulating the surface chemistry and optimize catalytic efficiency. We present a Pd-based catalyst in which the superficial strain of the Palladium nanocatalyst could be changed to improve its ORR efficiency in fuel cells by incorporating both iron and cobalt into the palladium lattice. Pt is also added to the synthesized Pd-based catalyst Pd_2CoFe/C, resulting in increased mass activity of 38 and 11.25 fold that of commercial platinum in 0.1M $HCLO_4$ and KOH solutions at 0.9V (**Figures 9** and **10**). Adding Pt to a Pd-based catalyst improved the ORR performance [38].

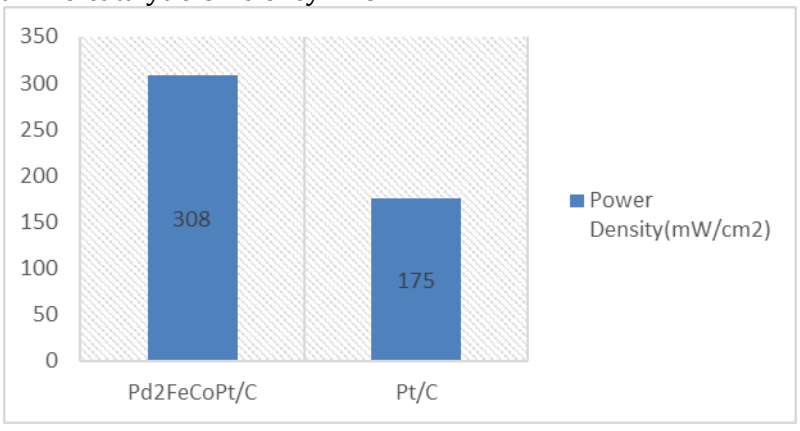

Figure 9. Power density of Pd-based catalyst compared with Commercial Pt

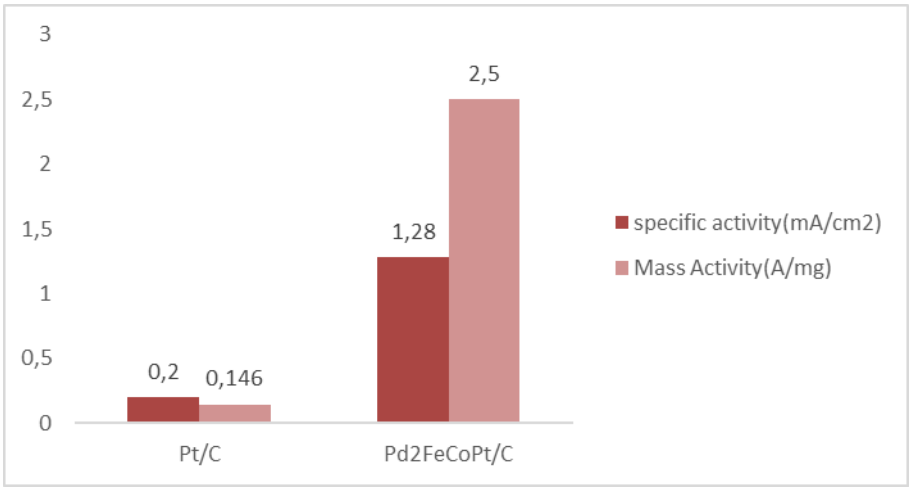

Figure 10. Mass activity and specific activity of Pd-supported catalyst compared with Pt/C

Another palladium based material Pd-Fe (**Figure 11**) bimetallic catalyst supported on carbon with different ratios of Fe (1:1, 2:1, and 3:1) was synthesized without adding any stabilizing agents. As a result, carbon-based palladium and bimetallic catalysts Pd-Fe have been developed with excellent ORR specificity and efficiency that is similar to commercial platinum Pt/C. These catalysts were made at ambient temperature with no thermal treatment [18].

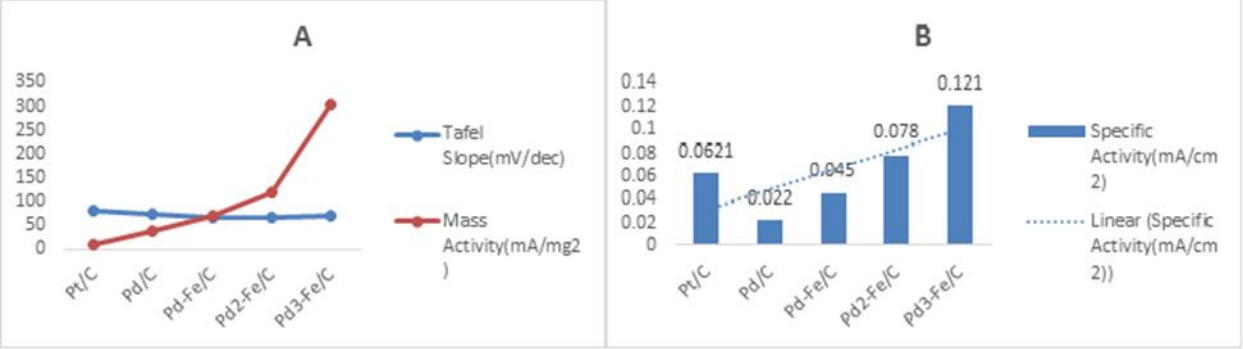

Figure 11. Tafel slope, mass activity, and specific activity of palladium-based materials compared with Pt/C in A and B

The third way is modifying Pd's electrical properties to locate suitable support systems that can boost palladium and palladium-supported electrode material sensitivity by allowing efficient electron bonding among both palladium and the assisted material. Pd–$W_{18}O_{49}$ is a type of composite nanomaterial that is made up of a palladium tetrahedron and tungsten oxide nanostructures. The result was surprising, reported hybrid nanomaterial (Pd–$W_{18}O_{49}$) exhibits extra-ordinary catalytic ORR activity and shows a higher activity to Pt in alkaline medium. Pd nanoparticles show a less catalytic activity toward ORR. The Pd alloys and its ORR activity are presented in **Table 2**. It was reported that the maximum catalytic activity and durability of Pd nanoparticles toward ORR is due to Pd-O bond [18].

9. *Cupper-Based Materials*

Due to its abundance on the globe, copper has been intensively explored in a wide range of domains, particularly glass electrodes and organo-catalyzed reactions. As in processes of glycolysis, H_2O_2 reduction, and methanol oxidation, Cu-based nanomaterials have proven to be excellent electrocatalysts. The early

experiments originally reported the ORR parameters for a substantial copper electrode [39]. It was claimed that a one-pot technique was used to manufacture subnanometer-sized copper aggregates with high ORR oxygen reduction reaction performance. The catalytic performance of copper clusters is also affected by the characteristic size of their cores. Cu_3N nanocuboids with a mean diameter of roughly 11 nanometer were made by using a simple one-pot procedure that could be adjusted by changing the amphiphillic molecules. Electrochemical experiments demonstrated that the as synthesized Cu_3N nanocubes had good catalytic activity for ORR in basic conditions. Though pristine copper oxides can catalyze the ORR reaction, they have limited electrochemical applicability due to their low electrical conductivity. Numerous investigations have shown that using graphene as a support optimizes the electrochemical behavior of copper oxides. Despite the fact that the Cu_2S nanoplates did not shows the great ORR activity as compared to the commercial platinum catalyst [39,40].

We illustrate a set of copper-palladium hybrids and copper-palladium nanostructured on huge active surface area graphite hybrids that can be used as efficient catalysts in energy technologies such as fuel cells. In an antacidic environment, all of the composites showed considerable ORR electrocatalytic performance. With starting voltage of 0.84 V and 0.91 V and charge density of -3.5 and -4.2 mA/cm² at 0.3 V, the Palladium-high surface area graphite and copper-palladium-high surface area graphite composites had the best results (**Figure 12**) [40].

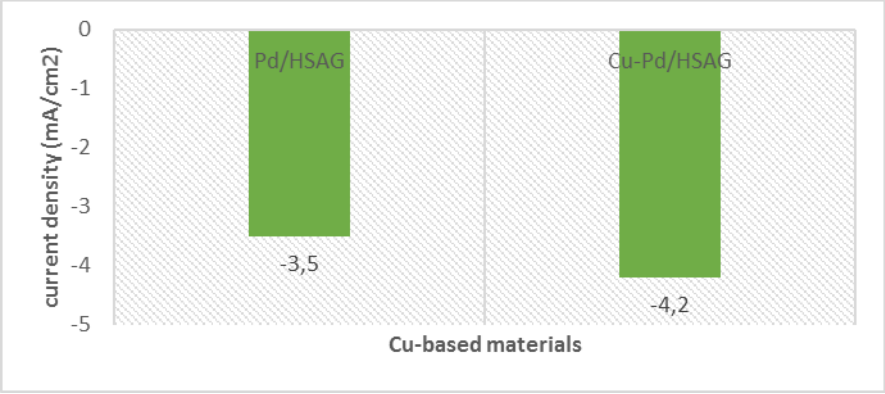

Figure 12. ORR activity of Cu-based catalyst is compared with Pd-based Catalyst

Table 2. ORR activity of different Pd-Alloys in fuel cell [41-52]

Catalyst	Morphology	Onset potential(RHE)	Mass Activity(mA/mg_{metal})	Specific Activity (mA/cm^2)
Ag-Co	Alloy	N.A	5.02	5.02
Ag-Pd	Random Alloy	-0.05	10.85	2.98×10^{-2}
Ag_4Sn	Intermetallic	0.6	759.31	50.76
$AuCu_3$	Intermetallic	0.7	2348	N.A
Au-Pd	Alloy	N.A	N.A	0.281
IrV	Random Alloy	N.A	N.A	0.231
Pd-Co	Random Alloy	0.9	0.14	0.07
Pd-Cu	Random Alloy	0.9	150	0.22
Pd-Fe	Random Alloy	0	159	0.312
Fe-Pd/Pd	Core Shell	0.9	105	N.A
Pd-Ni	Random Alloy	0.8	1100	N.A
Rh-Pd	Random Alloy	0.8	210	N.A

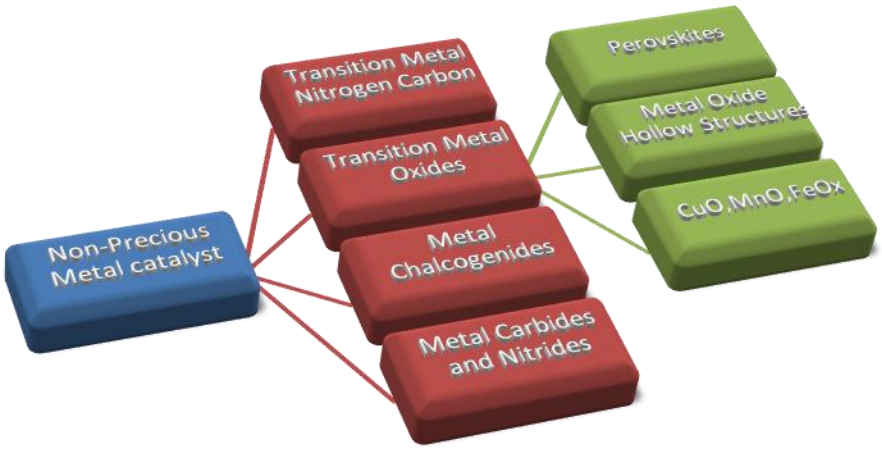

Figure 13. Non-precious metal catalysts for ORR

10. Non-Precious Metal Catalyst

Impetuses that accelerate the oxidation of fuel at anode and the reduction of oxidant at cathode separately are the primary prerequisite for more extensive utilization of power modules to make power. For PEM power modules, platinum, which was initially utilized by William Grove in 1839, is right now the main viable impetus [7]. Platinum is one of the most expensive to emulate metal in the world. It is not achievable to furnish a huge number of vehicles with platinum-based power devices from a monetary and natural angle. One solution is to use non-precious metal catalysts instead of Pt-based catalysts at the oxygen-reduction cathode, which would lessen the Pt content by a significant margin [53]. There are numerous ways to minimize Pt loading in cathodes without compromising their performance: Boosting the mass efficiency of platinum for oxygen reduction process through adding different metals or core-shell nano structuring, improving the mass-transport characteristics of platinum cathodes, and growing elite execution nonprecious metal impetuses for oxygen reduction process are largely considerable needs [11]. We depict a group of non-valuable metal impetuses that can coordinate with the viability of platinum derived frameworks at a lesser expense, making them reasonable for high energy unit present day auto power. The non-valuable metal electrocatalysts for oxygen reduction process incorporate non-pyrolyzed and carbon supported metal nitrogen compounds, transition metal chalcogenides, nitrides, carbides and perovskites (**Figure 13**) [10,54,55].

11. Transition Metal Nitrogen Carbon

Because of their minimal price, large catalytic activity, consistency, and resistance to the methanol cross-over impact, transition metal nitrogen carbon composites are the most attractive options among non-valuable metal ORR catalysts, and found that M–N–C has ORR catalytic activity and durability are nearly equivalent to commercially available Pt/C catalysts. Transition metal nitrogen carbon composites are effective for two reasons: (i) The performance of ORR is entirely dependent on nitrogen properties on the exterior of carbon supported catalysts and (ii) Nitrogen properties on the exterior of carbon-derived accelerators are mainly accountable for ORR performance, and nitrogen-groups serve as just a collaborating setting for iron and cobalt ions in which the ORR process takes place [56]. Transition metal macrocycle compounds have really been exploited for a multitude of scenarios, especially as an electrocatalyst in a various processes. A chelating ligand N4 in combination with a non-precious metal was reported as a feasible alternative for electrochemical reduction of oxygen. ORR activity has been investigated in a variety of

macrocyclic ligands with transition metal, including porphyrin and phthalocyanine. In each of these complexes, the Noble metal atom is uniformly enclosed by N4. The electron transfer from the electron donating core material to the diatomic oxygen p* orbital is expected to weaken the O-O bond, causing O_2 to be halved. In spite of the new distribution of a promising framework with 1.01 Volts open-circuit voltage and power thickness of 0.33 W/cm^2 greatest voltage at 0.2 MPa outright strain at 808°C, the effectiveness of fuel cells dependent on these materials. [53].

Transition-metal with nitrogen and carbon must all be contemporary at the same time to optiFmize ORR activity, according to the overall direction. We recently published a study focusing on materials obtained without heat treatment at first to synthesize non-valuable metal electrocatalysts of the high oxygen reduction catalytic performance and strong reliability and consistency. At the elevated temperature production of iron and cobalt catalysts, polyaniline (PANi) is used as a co-substrate to a carbon-nitrogen framework. Only PANI-derived compositions show the strong oxygen reduction catalytic performance with distinct efficiency and robustness in high-temperature non-valuable metal electrocatalysts. They demonstrated impressive ORR performance in a bitter environment with a E1/2 capability of 0.79 V, only 60milivolts variance from commercial platinum, greater sensitivity and specificity, and superior electrochemical stability. For the PANi supported metal-nitrogen-carbon composites, DFT calculations were used to ensure that the catalytic activities drop significantly in the sequential manner Co–PANI < Fe–PANI< CoFe–PANI. This is because of CoFe–PANI, a synergistic impact between heterogeneous metal atoms allows for more charged particle donation from active sites to adsorbed reduced oxygen dimers. As a result, these non-noble catalysts still have a hard way to go in order of ORR catalytic stability and activity. Non-platinum oxygen reduction electrocatalysts with high methanol endurance, such as iron-nitrogen supported carbon and cobalt supported carbon, are expected to be good choices for tackling the cost problem of fuel cell electrocatalysts, despite of extended kinetic energy of fuel cell commercialization. Iron-nitrogen supported carbon and cobalt supported carbon have lesser catalytic performance than Pt-based catalysts [3].

A set of non-valuable metal impetuses with iron, cobalt, or manganese as the transition metal and a reinforcing material of N-changed active carbon are produced using the following stages (**Figure 14**): (i) Topping of an N-rich polymer on activated carbons, (ii) Impregnation of the matching metal porphyrin on the N-polymer/activated carbon composite, (iii) Thermal decomposition at 800C in an inert atmosphere, and (iv) Dissolution of metals by means of acid to detach non-stable phases dramatic weight decline of iron-nitrogen supported carbon, cobalt-nitrogen supported carbon and manganese-nitrogen supported carbon specimens that recovered after step (ii) as the temperature inside the nitrogen surrounding was extended [57].

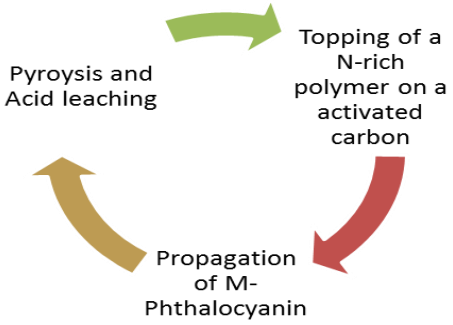

Figure 14. Steps involved in synthesis of non-valuable metal catalyst

The effectiveness of all of the catalysts in terms of ORR in acid medium was assessed by means of electrochemical methods. At typical capabilities between 900 and 700 mV, the catalytic efficiency follows the iron > Cobalt > Manganese trend in terms of oxygen reduction process beginning voltage and high specific density. Apart from all the type of transition metal, the amount of nitrogen and iron integrated into the carbon polymeric network reduces the thermal decomposition treatment, which leads to the production of genuine catalyst active surface area for the ORR. The NPMCs only show strong and stable electrocatalytic effectiveness for the oxygen reduction process after the carbonization phase. This process, which is likely aided by graphitic-N species, results in the creation of more ORR effective surface sites. To make pretty active ORR electrocatalyst, the transition metal must be carefully chosen. According to our results, iron produces more efficient electrode materials than cobalt and manganese for the oxygen reduction process. In this study, ortho, meta, para-phenylenediamine/iron/carbon forerunner is used to make iron-based ORR catalysts through thermal treatment approach [58].

A facile heat treatment using iron salt, graphitic carbon nitride (gC_3N_4) as precursors, and chemically whittled down graphene yields iron-nitrogen-functionalized graphene (FeNG) as a NPMCs. When comparing the electrocatalytic performance of the synthesized catalysts to that of Sequential scanning cyclic voltametric tests on pristine graphene sheets show that the iron-nitrogen-functionalized graphene catalyst has a higher positive beginning potential and greater reduction specific densities, indicating that FeNG catalyst has a better ORR activity than pristine graphene. The FeNG, in particular, has the maximum peak power thickness of 1150 mW/m^2, which is 2.1 times significantly greater than the commercial platinum (561.1 mW/ m^2) and considerably higher than the Pristine Graphene (109 mW/m^2). These findings suggest that in practical MFC applications, the FeNG catalyst could be a fine replacement for the more expensive platinum catalyst [59,60].

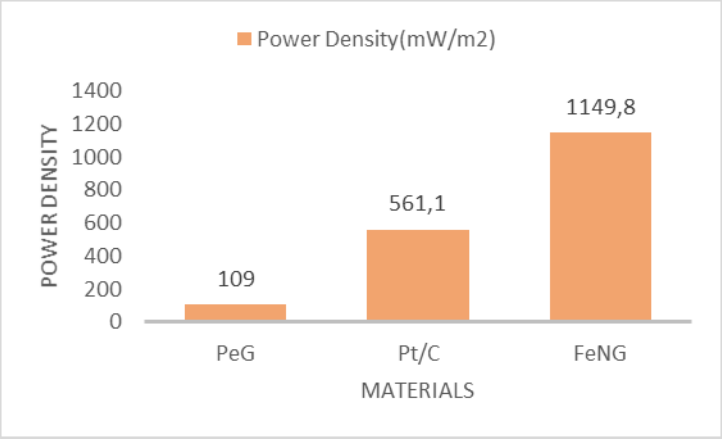

Figure 15. Power density of iron functionalized nitrogen supported on carbon compared with Pt/C

Nanosized Mn(III) oxide was used to make a thin layer counterpart. The bifunctional oxygen reduction performance and activity of this plentiful and reduced price catalyst is equivalent to the best renowned precious metal catalysts like platinum, ruthenium, and iridium [61]. In an alkaline exchange membrane, catalyst like this could be used as the oxygen cathode where oxidation reduction reaction takes place. A simple process for preparing thin layer like cobalt-nitrogen-graphene composites (Co-N-G) has been reported that function like an extremely active and potent NPMCs for the oxygen reduction reaction. Polypyrrole/graphene oxide (PPy/GO) nanostructures have been prepared at room temperature through in-situ polymerization. Cobalt (II) nitrate as a precursor was then heat treated instantly into the PPy/GO blends to create the Co–N–G composites. The cobalt-

Nitrogen-Graphene nanocomposites had exceptional electrocatalytic activity toward ORR, equivalent to commercial platinum, with greater onset potential, remarkable tolerance to the presence of methanol, and absolutely superb alkaline environment consistency. They were consider as the modern and more explored non-precious metal (NPM) ORR electrocatalysts for electrochemical applications because of these properties [62].

12. Transition Metaloxides (TMO_x)

Because of their outstanding stability and catalytic efficacy, transition metal components such as TMOs have been widely studied as ORR catalysts in alkali environments. TMOs (transition metal oxides) are a material family that has sparked a lot of interest in the research community for ORR. These mixtures are comprised of change metal oxides from the d-block, which may be single or blended metal types [63]. TMOs are appropriate to electrocatalytic purposes since they might show a wide scope of valence states and glasslike stages that can be changed or altered to maximize effective site association with the ORR items [64]. The minimum cost TMOs are easier to acquire and control than other transition metal compounds that increase their demand. On the other hand, TMOs have also some downfalls. Transition metal oxides are semiconductors, they must be made more conductive before they can be used as electrocatalysts. Previously, TMOs have been found to be very effective when combined with different outstanding conductive precursors, including nanomaterials, carbon-supported materials, and highly conductive polymers. Because of their varied oxidation states and high electrical conductivity, metal oxide from d-block metals are promising aspirants for non-platinum oxygen reduction electrocatalysts [63]. CoOs have been lauded as one of the most encouraging electrocatalysts for power device processes when contrasted with other transition metal oxides. It is modest, high surface-to-volume proportion with synthetically stable situations, and higher explicit potential make it appropriate for energy-related gadgets (890 $mAhg^{-1}$). Co_3O_4 has precious stone construction and possess tetrahedral and octahedral opportunities, separately for Co^{2+} and Co^{3+}. A crossover material comprised of Co_3O_4, 3D nitrogen-functionalized graphene nanofillers and nanocrystalline, named Co_3O_4/N-GAs, was integrated to test ORR. The catalyst was made by using the low-cost precursors and a one-pot hydrothermal technique. The reaction is clearly carried out in a four-electron reaction mechanism with a greater current density and a long lifespan. TMOs with a variety of exposed facets were also successfully synthesized. The forms of nanorods, nanocubes, and nanooctahedrons with different exterior surfaces 110, 100, and 111 were reported previously. The performance sequence of ORR nanocrystalline is Co_3O_4 ‹ Co_3O_4 –NR ‹ Co_3O_4 –OC indicating that the catalytic performance of the Co_3O_4 111 surface was the highest among all others [62].

ORR electrocatalysts have also been discovered in TMOs such as titanium oxide, niobium oxide, and tantalum oxide [64]. In recent years, another category of oxides, the perovskite oxides with the general formula ABO_3, has attracted a lot of attention. Perovskite materials with metals at effective B- site are substitute electrocatalysts for reduction of oxygen to water only through the ORR activity [65]. Essential cations like La^{3+} are found in the transition metal oxides with the perovskite structure; oxides of these particles are unsound in solid corrosive arrangements. Therefore, basic arrangement has been utilized to investigate perovskite metallic oxides as permeable cathodes. ORR activity could be influenced by the number of transition metal d-electrons, the robustness of the M–OH bond, and its impact on rate-determining processes involving intermediates [7, 17, 66]. However, insufficient knowledge about ORR reaction mechanism and the material characteristics that influence electrocatalytic activity still exists. (La,Sr)A(Ni,Mn)B(Ni,Ru)B′ O_6 (LSNMR), a dual perovskite with particular cationic species in the A, B, and B′ positions, has been reported. The contrast among the potential estimated at 1 mA/cm^2 for the ORR has a striking bifunctional record of 0.83V. In basic medium, this bifunctional LSNMR electrocatalyst has phenomenal ORR and OER performance. The

0.94V ORR beginning potential is one of the most amazing so far for ORR-dynamic perovskites in antacid conditions. The oxygen reduction mass action of LSNMR is 1.1A/g¹ at 0.9V and 7.3A/g¹ at 0.8V. Density functional theory interpretations showed that the maximum ORR performance of LSNMR is linked to the existence of effective Mn positions due to the strong symmetry of the respective reaction mechanism on those position [67]. In addition, the catalyst is relatively durable during Oxygen reduction cycling. Another perovskite oxide based on Ba, Sr, Co, Fe, and O (BSCF5582) is being praised a di-functional electrocatalyst candidate for oxygen reduction process and oxygen evolution process [66].

Copper oxides and cobalt oxides are good non-valuable metal electrocatalysts for oxygen reduction process because of their large specific surface to volume ratio, varied valence states, and chemical inertness. Still, due to its low conductivity and catalytic activity, it is not suitable for broad use. To improve CuOx's electrocatalytic capabilities, mixing it with carbonaceous material is a viable option [68]. It was reported that Cu^{2+} ions have a stronger tendency for forming stable complexes with N-based ligands. CuO and N-rGO are therefore combined to form a nanocomposite, CuO/N-rGO, with high ORR activity. With a 4 electron transfer throughout the reaction, this nanocomposite may rapidly decrease HOO^- intermediate, leading in a high current density and a higher positive start potential [60, 69]. Catalysts made of manganese oxides (MnOx) are another potential type of cathodic material for alkaline fuel cells. They are cheap, plentiful, and safe for the environment, and they come in variety of shapes and sizes, several of them have been reported to have significant electrocatalytic performance for the 4e-lessening of oxygen. Carbon electrodes, the most common substrate for oxygen reduction facilitators in fuel cell cathodes, have long been acknowledged as catalysts with high inherent action for the electrical reduction of oxygen to peroxide. In this way MnOx is supported on carbon electrodes. We report the ORR activity of bare graphene and graphene supported MnOx electrodes in air as a function of thermal treatment over a range of temperature. In our experiments, Mn_3O_4 was discovered to be a MnOx phase with 4e- reduction of oxygen for the ORR performance and an approximated specific density of 3700A/cm² at 0.75V vs. [RHE], a value that is incredibly fierce with the effective precious and nonprecious electrocatalysts for the oxygen reduction process in core. A simple technique was used to make another $Mn_2O_3/LiNi_1/3Co_1/3Mn_1/3O_2$ composite electrocatalyst. Hybrid electrode catalyst are synthesized having a high porosity and a large surface to volume ratio. The hybrid electrode catalyst has an extraordinary capacity for oxygen sorption. The NCM-2 ($Mn_2O_3/LiNi_1/3Co_1/3Mn_1/3O_2$) composite material has outstanding electrocatalytic properties for oxygen reduction process, as well as improved stability. As Oxygen reduction triggers, a new class of transition metal oxides called CoxOy, MnxOy, FexOy, and others is gaining traction [70].

Iron is an inexpensive, abundant metal with greater ORR selectivity, making it a viable substitute for precious metal catalysts. Iron is thought to be particularly effective and energetic in ORR activities. Due to their reduced oxygen reduction action, iron oxides, on the other hand, have a limited universal applicability in fuel cell technology. During their amalgamation, uncontrolled development and accumulation happen, bringing about a misfortune in execution. A decent method for conquering these deterrents is to use a conductive help, and carbonized materials. ORR is effectively catalyzed by the created nano-Fe3O4/graphene composite. The improved properties are said to be due to the beneficial synergistic bonding impacts among both iron oxide and graphene [71].

Another material for ORR in energy-related applications is metal oxide porous frameworks, which have a greater surface area, light weight, and the maximum loading potential. Transition metal oxides with porous frameworks, which act as oxygen-related catalysts, have a low over potential, a fast reaction rate, and high stability. Templating procedures make it simple to create hollow structures. It was reported that $ZnCo_2O_4@NiCo_2O_4$ core–sheath nanowires with

a hierarchical structure have also been produced uncontrollable an amalgamation of easy electrospinning and a simple co-precipitation method. The onset potential of the hierarchical structure is analogous to that of conventional platinum catalyst, but it is far more stable. It is hierarchical core sheath architectures improve reactivity and ion transport significantly. For Fe-based spinels, porous $CoFe_2O_4$ nanostructures with a distinguishable bimodal microporous structure were described. This 3D hierarchical hollow structure is beneficial for oxygen transport and the development of a three-phase reactive action interface in metal–air batteries. As a result, there will be a higher ORR activity and an improvement in stability [72]. A wide range of highly effective modern catalysts have been produced by dumping massive volumes of transition metal oxides like manganese oxide, cobalt oxide, nickel oxide, copper oxide and iron oxide onto nitrogen-doped carbon nanotubes for di-functional catalysis in basic medium. The metal oxides were distributed onto functionalized CNTs using an enhanced impregnation technique. This new method allows for the production of di-functional nitrogen-doped CNTs and a uniform distribution of MOx on the CNT wall surfaces. The 50wt% MnO_2-CNT catalyst is the most effective ORR electrocatalyst in this series, with a E1/2 prospect of 0.84V at a specific density of -2.1 $mAcm^{-2}$ and a beginning voltage at 0.98V vs reversible hydrogen electrode [72-74].

As oxygen decrease impetuses, we gathered cobalt porphyrins and d-metal oxides on gold and carbon or graphene cathodes. After porphyrins were momentarily impregnated, d-metal oxides like cobalt oxides and nickel oxides were set utilizing either unconstrained or electrochemical accumulation techniques. The oxygen reduction activity results show that co-deposited d-metal oxides increases the movement of cobalt porphyrin towards oxygen reduction process. The CoOxCoP/Au impetus was more dynamic in working with oxygen reduction than the NiOxCoP/Au impetus [75].

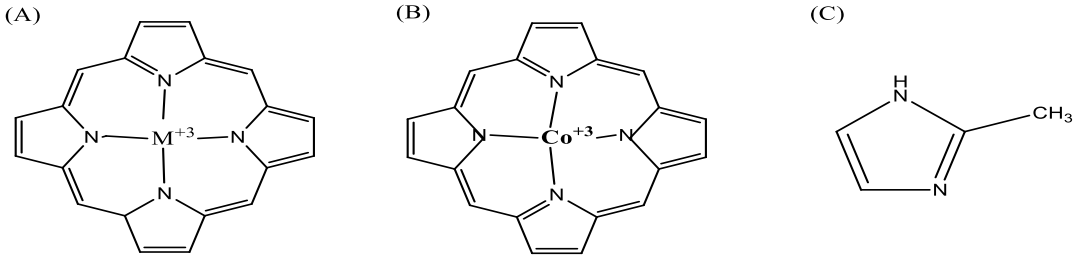

Figure 16. Structure of (A) porphyrin (B) cobalt porphyrin (C) 2-methylimidazole (carbon building block for ZIFs)

13. Transition Metal Chalcogenides

Over the last period, d-block metal chalcogenides M–X, where metal is cobalt, ruthenium, rhenium, rhodium, and X is sulphur, selenium, or telenium have been studied as the ORR electrocatalyst. Baresel *et al.* explored the cathodic oxygen reduction response on chalcogenides of d-block metals in 1974 and found that the cobalt-Sulphur and cobalt-nickel-sulfur frameworks had the most noteworthy electrocatalytic execution, with 2250 mA/m^2 or 1000 mA/g^1 at 70 °C and beginning capability of 600 mV in 2M H_2SO_4 electrolyte, individually. At the point when the distinction in energy between the 2p orbital of oxygen and the most populated d-orbital of the metal of the sulfide diminishes, the action in the relating intensifies drops in the order of sulphur > selenium > telenium [76,77].

The early transition metal chalcogenides electrode material have been proposed as possible non-platinum oxygen reduction electrocatalysts due to the advantages of less price, powerful ORR efficiency, excellent methanol resistance, and ease of fabrication. Hydrothermal/solvothermal soft synthesis, only one forerunner soft synthesis, one-pot synthesis, template assisted synthesis, and Kirkendall effect are the most commonly used early transition metal chalcogenides methods. Cobalt

sulphides have been studied as the most active Oxygen reduction electrocatalyst among the chalcogenides acidic solution. Through a 4e-ORR pathway, the electrocatalytic efficiency of Co_9S_8 is assumed to be similar to the platinum, and S-S offers a sorption position for Oxygen after O_2 bond cleavage. For ORR, a ternary effective composite Co_9S_8–N–C catalyst was synthesized in alkaline medium. The ORR activity of Co_9S_8–nitrogen supported on carbon catalysts is much sophisticated than that modern platinum catalyst in 0.1M NaOH solution [76]. This study designed a new trinal non-vluable metal chalcogenide, rest on tungsten and cobalt in an effort to increase ORR electrocatalytic activity. While these two non-precious metals are sluggish against the ORR and unbalanced in a sharp solution, electronic characteristics changed by a chalcogen atom such as selenium are predicted to expand their constancy and efficiency. In an acidic environment, the ORR catalytic efficiency, constancy and durability of the synthesized ternary tungsten-cobal**t-**selenium chalcogenide was assessed. The link among the altered electronic characteristics and the electrocatalytic efficiency was investigated which shows an effective ORR electrocatalytic efficiency [77]. Another significant class of chalcogenides is u-based chalcogenides.

14. Transition Metal Carbide and Nitride

The d-block metal nitrides with elevated electrocatalytic efficiency, stability, and enduring robustness are also hunted by oxygen reduction electrocatalysts. To make carbon-assisted Co-N, the reflux and temperature treatment were used. It is equivalent to traditional platinum catalyst in terms of catalytic efficiency, but it overtakes Platinum in terms of stability. Zirconium oxynitride and tantalum oxynitride were discovered to have a reasonable ORR performance and outstanding chemical resistance in sulphuric acid. The commutative properties of Molybdenum nitride and dimolybdenum nitrides were demonstrated.[78]. To make a complex catalyst, dual d-block metal nitride nanoparticulates titanium-cobalt-nitride were placed on nitrogen-incapacitated reduced graphene oxide. The electrocatalysts demonstrated the excellent oxygen reduction activity in an antacid media. The maximum E1/2 capacity of the Ti-Co-Np/N-rGO catalyst was 0.902 V against RHE which was 30 mV significantly high than the marketing Pt/C catalyst, and the output specific density was 2.51mA/cm^2 at 0.9V against RHE. The oxygen reduction action of d-block metal nitride-nitrogen doped-reduced graphene oxide was essentially advanced than that of metal nitride or N doped reduced graphene oxide alone showing a huge synergic movement between the two materials. The ORR activity was excellent, and the reaction went through a roughly 4e-cycle [79]. Nanosized ZrN was produced using the urea glass approach technique, and the ORR efficiency was established to be sophisticated than that of the conventional platinum catalyst. The ZrN nanostructures were also found to have an extraordinary efficiency analogous to that of the modren commercial Pt catalyst [67].

Cobalt-tungstum supported on carbon matrix treated with active NH_3 was found to be structurally oxynitride. By looking at the strong correlation among both specific density and innumerable nitrogen-holding classes, they discovered that d-block metal nitrides and pyrrolic nitrogen both seem to be effective agents for the ORR catalysis. It was found that cobalt-molybednum oxynitride, is preferable in the ORR catalytic reactions in basic environment because of high beginning voltage 0.918V against reversible hydrogen electrode and reasonable in acidic environment. The metal carbides with electrical properties and consistency in acidic conditions had been previously used as electrocatalyst support systems for ORR by adjusting the d-band center to the ideal location, with tungsten carbides being the most commonly used. They have now established themselves as ORR catalysts. Molybdenum is one more metal whose carbide has electronic characteristics compared with platinum, resulting in a synergetic action amongst the Platinum catalyst and the molybdenum carbide backing. The microwave-assisted technique was used to successfully produce well-dispersed Mo_2C particles of 3 nanometer size on the surface of carbon nanotubes. The efficiency of the conventional platinum over molybdenum carbide support on

carbon nanotubes revealed a high electrochemical effective surface area to volume ratio and a greater oxygen reduction beginning voltage. ZrCN, TaCN, and NbCN are metal carbo-nitrides with strong oxygen reduction efficiency, principally after half-done oxidation, with ORR onset potentials of 0.97, 0.9, and 0.89 V, respectively [78].

15. MOFs-Based Materials

Metal-organic frameworks based catalyst (**Figure 17**), comprising pure metal organic frameworks, their composites, and associated parent materials, are appearing as distinctive electrode materials for ORR activity in the perspective of alternative sustainable sources of energy [13]. MOF derived electrocatalysts offer unique possibilities to speed up the slow oxygen reduction process at the cathode surface in energy storage devices such as fuel cells due to their changeable compositional content and morphologies. The precious metal catalysts are recognized as the excellent ORR electrocatalysts with 4e- route (**Figure 18**). Unfortunately, because of its shortage, high cost, and poor robustness, platinum is not extensively employed in renewable energy systems. Given these limitations, developing earth-copious, high efficiency, and long-lasting alternatives is indeed a necessary but tough task [80]. Metal-organic networks are a new form of porous structure with excellent crystallinity and broad range ordering that are linked by coordinate covalent bonds between metallic ions and organic connectors [81].

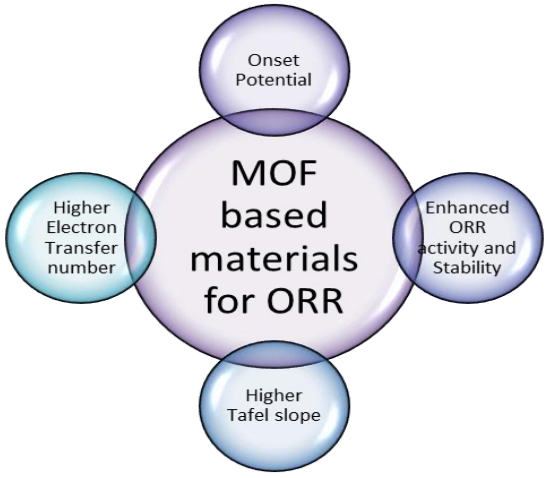

Figure 17. ORR activity of MOF's based materials

Depending on the chemical makeup, MOFs derived electrocatalysts are grouped into three types: crystal-clear metal organic frameworks, MOFs based composite materials, and their analogues [30]. Metal organic frameworks with porous channels and accessible sites with redox ability may have a greater active site usage than traditional heterogeneous catalysts. However, their electrocatalytic uses are severely limited because of inadequate electrical conductivity and chemical stability [30, 81]. Metal organic frameworks can be combined with novel functional nanomaterials such nano-carbon based materials and nanostructured materials (nanoparticles) to obtain excellent electrocatalytic performance [31, 82]. Another simple and practical way is to use immediate calcination or indirectly post-treatments to convert metal organic framework materials or MOFs-hybrids to inorganic hybrid materials [83]. Because of their structural and compositional advantages, MOF derivatives often have a huge surface area, outstanding electrical permeability, and excellent chemical inertness [80, 81, 84]. This mini-section starts with an explanation of ORR and Metal organic frameworks, and then divides MOFs-based electrode materials into categories depending on their ORR potential. In constructing MOF-derived oxygen reduction process

electrocatalysts, the importance of synthesis technique, composition, shape, geometry, electrocatalytic effectiveness, and reaction conditions is addressed. Non-noble metal-centered electrocatalyst, specifically iron and cobalt centered catalysts have already been investigated for the effective ORR electrocatalysis because precious metals like Pt, Ir, and Ru are in short supply and expensive. The ORR performance has previously been observed in MOF-based carbon materials with atomic scale distributed metal sites, metal based nanostructured materials, and composite based nanoparticles, all of which have been discussed in this section.

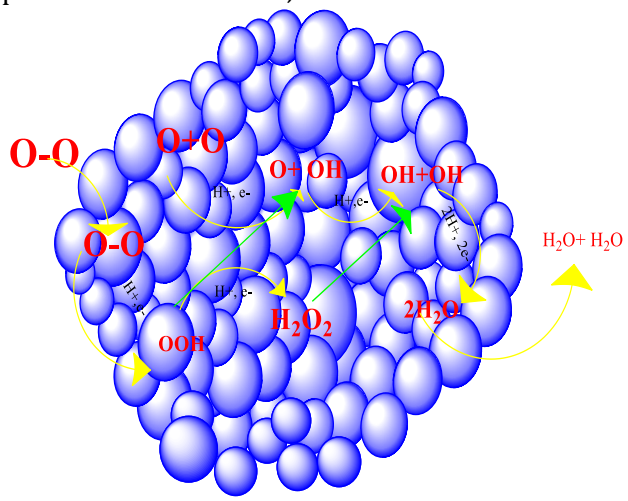

Figure 18. ORR mechanism in MOFs based Materials

The zeolitic imidazole frameworks, or ZIFs, are one of the more well-studied MOF groups due to their structural resemblance to zeolites, a family of aluminosilicate minerals. 2- methylimidazole is a typical carbon building block for ZIFs, with a structure similar to that illustrated in **Figure 16** (C). When zinc is doped into the MOF, it becomes ZIF-8; when cobalt is doped into the MOF, it becomes ZIF-7 [85].

To replace Pt-based materials, non- precious metal based catalyst with greater and optimum ORR are desperately needed. The metallic cobalt and nitrogen co-doped carbon based catalyst were produced by using a standard thermal decomposition technique, and alloy of two metals zinc and cobalt based ZIF was created by using polypyrrole and polyaniline copolymers as precursors. The acquired MOFs composite electrocatalyst ZIF-ppy-pani-750 has a greater ORR efficiency than bare ZIF-750 (**Table 3**), which is similar to the previously described conventional platinum electrocatalyst and other ORR electrocatalysts (**Figure 19**) [86].

Table 3. ORR activity of MOF-based catalyst and commercial Platinum catalyst

Materials	Onset Potential (V)	Current Density (mA/cm^2)	Dynamic Current Density (jk) (mA/cm^2)	Electron Transfer Number(n)	Tafel slope (mV/dec^{-1})
ZIF-750	0.90	4.69	12.22	3.64	52.5
ZIF-ppy/PANI	0.93	4.99	24.94	3.82	43.6
Pt/C	0.94	5.07	17.45	3.95	66.9

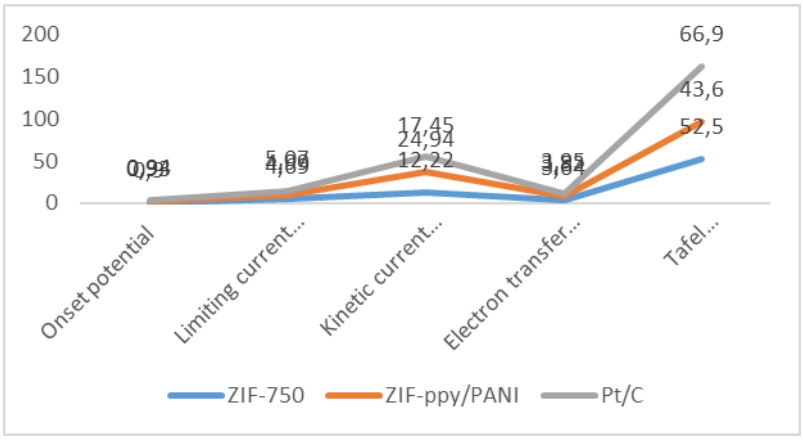

Figure 19. Comparison of ORR activity between MOFs and Pt/C

By using a one-pot approach, we demonstrate how to produce hollow carbon catalysts doped with nitrogen, cobalt, zinc, and nickel. The effective metal components are combined with 2-methylimidazole to create a zinc centered zeolitic imidazolate framework with nickel and cobalt as a dopants for the formation of nickel, zinc, cobalt, and nitrogen multi-doped porous carbon via thermal annealing, in which compartments and pores are formed naturally to zinc volatilization at extreme temperatures. In particular, as-synthesized nickel cobalt zinc and nitrogen multi-doped porous carbon exhibits advantageous ORR electrocatalysis at 0.864 V half-wave voltage and restricted oxygen reduction current density of 6.40mA/cm$_2$, outstanding resistance to methanol and enhanced long-term consistency. Metal air batteries especially Zn-air batteries of nickel, cobalt, zinc, and nitrogen multi doped porous carbon as the cathode material also has an extremely high open circuit voltage, high detection limit, power density and reliability, indicating that it could be useful in real energy conversion devices. However, in the sequence zinc and nitrogen doped porous carbon (5.20 mA/cm^2, 0.736 V) < Cobalt-zinc-nitrogen doped porous carbon (6.03 mA/cm^2, 0.848 V) < Nickel-zinc-cobalt, and nitrogen multi-doped porous carbon (6.40 mA/cm^{2,} 0.864 V), the limiting current density (JL), and E1/2 increases, indicating that ORR efficiency of highly porous nanocarbon catalysts improves as doped metal elements starts rising (**Figure 20**). Tafel slope has long been recognized for its importance in revealing reaction mechanisms, particularly in elucidating rate-determining stages. The nickel, zinc, cobalt, and nitrogen multi-doped porous carbon has the smallest Tafel slope (90 mV/dec^1) that is comparable to that of commercial platinum, revealing that nickel, zinc, cobalt, and nitrogen multi-doped porous carbon has higher efficiency and stability than the other two microporous carbon catalysts [87].

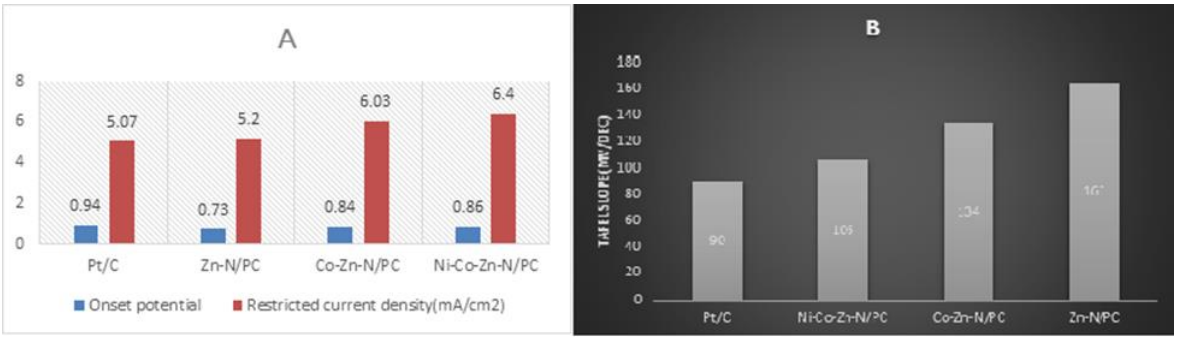

Figure 20. Onset potential, current density of different MOFs materials are compared in A and Tafel slope in B

The cobalt *p*-phenylenediamine coordination compound was created by using *p*-phenylenediamine as an organic binder, and it was then examined further as a novel ORR electrocatalysis. *p*-phenylenediamine with multiple amino groups was chosen as an organic binder to bind with cobalt and form a coordination compound cobalt *p*-phenylenediamine due to the high inclination of its -NH_2 molecule to interact with inorganic cationic species. Cobalt *p*-phenylenediamine compound had bisecting nanolayers and resembled a flower after a simple hydrothermal treatment. Even more, the patterning of the matched products was totally retained after decomposition at extreme temperature and acid etching in 0.5 M H_2SO_4. In contrast to other approaches, by using *p*-phenylenediamine as the only nitrogen and carbon organic binder has the clear advantage of being cheap, easy to make, and appropriate for large manufacturing exhibiting great repeatability. The novel cobalt and nitrogen doped carbon electrocatalyst has the potential to be a worthy substitute for platinum electrocatalysts due to its high electrocatalytic efficiency and impenetrability (**Figure 21**) [22].

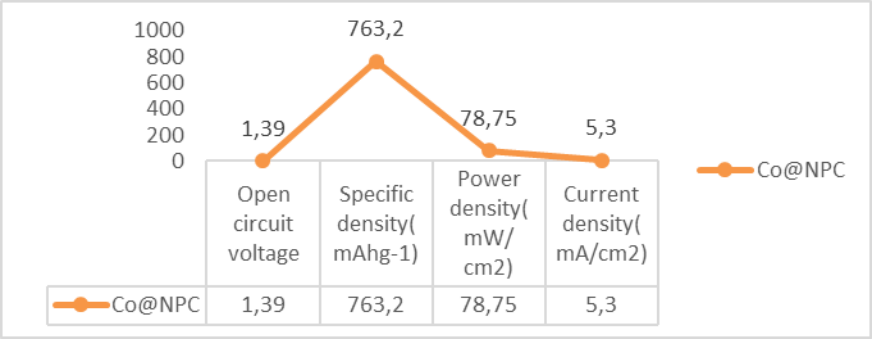

Figure 21. ORR activity of a MOFs based Co@NPC

Phosphorus, a group of heteroatom like nitrogen with chemical properties compared with nitrogen has diverted the attention. Because of the difference in diameter and electronegativity, phosphorus-doping of graphene sheets differs significantly from *N*-doping [88]. Phosphorous-doping of carbonaceous material has better electron-donating properties, great O_2 adsorbent, and strong oxidizing agent than the N atom, indicating that it is a feasible ORR electrocatalyst. Even so, in carbon Phosphorous-doping, no agreement exists on the reaction sites. Mesoporous carbon supported materials with heteroatom dopants have subsequently gained considerable attention because of its remarkable catalytic efficiency for an oxygen reduction process. MOFs are anticipated to improve ORR cyclic stability and catalytic performance by forming noble metals like iron and cobalt doped with a substituent like phosphorous and nitrogen. We present a bunch of new iron and cobalt integrated in phosphorous-doped porous carbon materials with excellent ORR efficiency using an in-situ combustion technique. The electrocatalytic efficiency and stability was evaluated by the combustion temperatures and quantities of the two metals. Iron and cobalt integrated in a phosphorous doped moderately permeable sample burned at 9000 °C offers the highest electrocatalytic strength and endurance because of the combined impact of the two noble metals. Cobalt and iron integrated in Phosphorous doped extremely microporous materials appear attractive as electrode materials to replace platinum catalysts in energy storage devices like fuel cell, according to electrochemical testing. The FCPA-900 sample, which was directly analogous to the commercial platinum catalyst, had the highest electrochemical performance of the three samples. FCPA-900 is a possible future electrocatalyst for fuel cells that could replace Pt-based catalysts (**Table 4**) [88,91,92].

Table 4. ORR activity of FCPA at different temperature and compared with commercial platinum catalyst

Samples	Onset potential	Current density (mA/cm^2)	Electron transfer number	Tafel slope(mV/dec)
FCPA-800	0.84	4.80	3.26	98
FCPA-900	0.87	5.68	3.72	90
FCPA-1000	0.88	4.34	3.04	97
Pt/C	0.96	5.25	4.00	75

We made a MOF-74 substrate with different metals species of iron and manganese and a cheap organic reagent dihydroxybenzoic acid, which we then bonded with melamine and heated up at 800°C under noble gas flow rate to make fundamental electrocatalysts. Iron and manganese bimetallic nanoparticles are encapsulated in nitrogen doped carbon nanotubes in all of these electrocatalysts. With an electron transfer total count of 3.95, Fe_3Mn1/N-CNTs-100 outperforms Pt/C catalyst in terms of ORR strength as well as consistency, implying a 4e-transfer mechanism. Fe_3Mn1/NCNTs-100 has the best ORR effectiveness, outperforming Pt/C catalyst, with a positive E1/2 of 0.865 V and a jk of 1.447mAcm² at 0.9V onset potential (0.855 V, 0.946 mAcm²) [93].

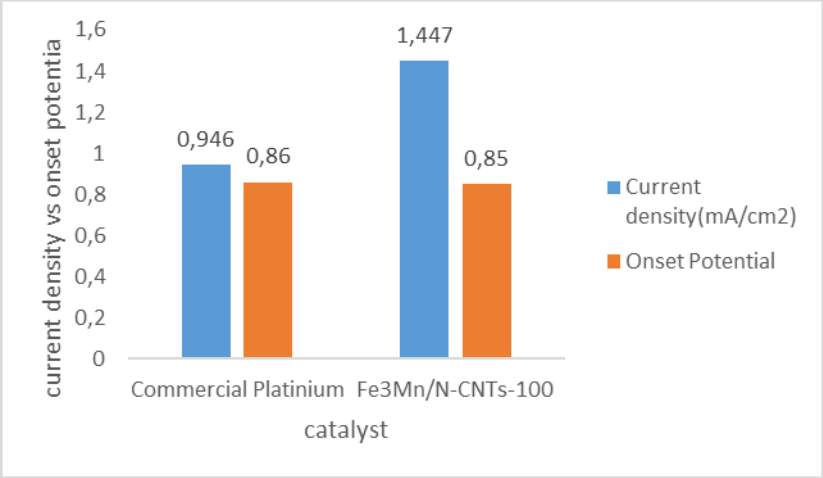

Figure 22. ORR activity of bimetallic iron and manganese based MOF-74

The thin and abundant magnesium ion was utilized as just a substituent in a cobalt-metal organic framework to produce a bunch of magnesium cobalt bimetallic metal organic framework. Such thin magnesium ion not only reduces framework intensity, improving the fuel adsorption effectiveness of the resulting magnesium cobalt bimetallic organic framework, but it also renders them appropriate components for the carbonization of ordered carbon nanotubes containing nanoporous carbon molecules under extremely light conditions. The produced ordered nanocarbons demonstrate a higher ORR efficiency that is exactly similar to the traditional platinum catalyst after further loading with Nitrogen or Sulphur heteroatoms. In the future, more Mg-containing bimetallic MOFs will be synthesized, and their possible uses as active carbon antecedents will be explored. There was no significant performance degradation when adding methanol to the carbon-900–nitrogen/sulphur. The ORR catalytic activity dropped considerably when methyl hydroxide was introduced to the traditional platinum. In terms of ORR catalytic activity, robustness, and

resistance to methanol crossover, nitrogen and sulphur co-doped highly permeable carbons of carbon 3-900–nitrogen/sulphur surpassed the conventional platinum catalyst (**Figure 23**) [94].

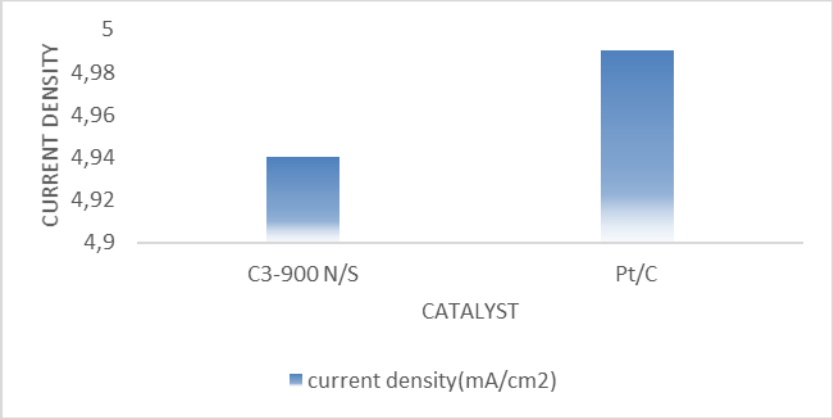

Figure 23. ORR activity of nitrogen/sulphur co-doped with carbon 3 compared with traditional platinum catalyst

According to reports, a simple corrosion, pyrolysis, and replacement approaches are successfully used to produce cobalt, Iron, and nickel co-doped and nitrogen rich porous carbon Co-Fe-Ni/NC for ORR electrocatalyst. The framework of polyvinylpyrrolidone-zeolitic imidazole framework-8-zeolitic imidazole framework-67 may be peeled by Ni^{2+} during the hydrolysis process, and the resultant zinc metal can be eradicated by iron (II) through a replacement reaction methodology. The addition of iron and nickel improves the graphitization amount and specific active surface area of the electrocatalyst. Electrocatalytic performance of as-synthesized samples was also thoroughly investigated. The ORR efficiency of the electrocatalyst may be significantly enhanced by iron and nickel. Compared with cobalt-zinc co-doped nanocarbon, Cobalt-iron-nickel co-doped nanocarbon has a higher oxygen reduction response, a higher contemporary thickness of 2.593 mA/cm^2, and a higher onset voltage of 0.914 V. In addition, cobalt-iron-nickel co-doped nanocarbon effectively prevents oxygen reduction degradation, resulting in good long-term operating stability (**Figure 24**). At 0.85 V, cobalt-zinc co-doped nanocarbon has a minimum cutting efficiency of $0.608mA/cm^2$. When contrasted to oxygen reduction reaction, cobalt-zinc co-doped nanocarbon has an onset potency of 0.812 V. The Ni-doped CoZn/NC exhibits a larger current output of $0.950mA/cm_2$ and a higher onset voltage of 0.826V than the well-known Ni-doped CoZn/NC. Cobalt-iron co-doped nanocarbon and Cobalt-iron-nickel co-doped nanocarbon, on the other extreme, have limiting current densities of 2.05 and 2.593 mA/cm^2, respectively [95,96].

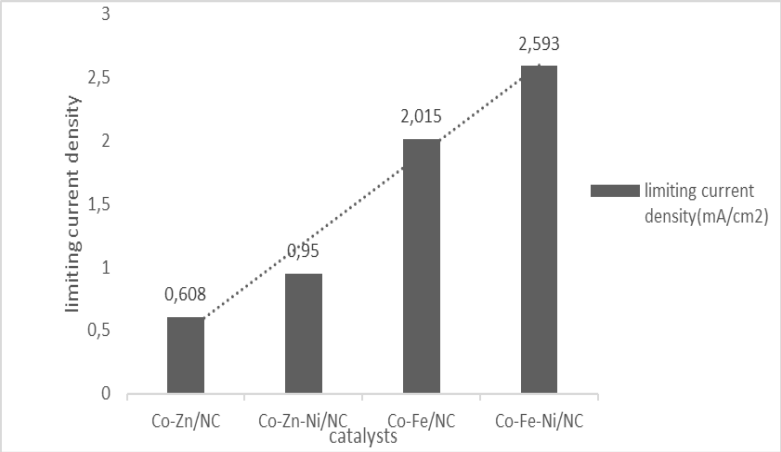

Figure 24. ORR activity of MOFs based ORR catalysts

Nanoporous carbon material is co-doped with nitrogen, phosphorous and Sulphur that results in ternary electrocatalyst called NPS-CMOF-5 for ORR have also been produced by using MOF-5 as a soul framework. The nitrogen, phosphorous, and sulphur forerunners were dicyandiamide, triphenylphosphine, and dimethylsulfoxide, respectively, and continuous doping of nitrogen, phosphorus, and sulphur results in the formation of carbon composites. When heteroatoms (N, P, and S) are loaded into carbon skeletons, the porous structure of these materials changes, and it's possible that some of the small pores in heteroatom-doped materials are sintered, resulting in a reduction of small pores and a boost in large pores, resulting in different ORR activities (**Figure 25**). Boron-doped (B-doped) carbon electrocatalysts have also been used in ORR in recent years. Boron has one less electron than carbon and is hence less electronegative. Boron is a suitable choice because it generates an electronegativity difference in carbon compounds in the same way that nitrogen does. When electron rich nitrogen and electron deficient boron are doped into the carbon lattice at the same time, the electronic attributes of the surface of the electrode are considerably altered, which has a considerable impact on ORR efficiency. The increased electrocatalytic effective sites for the ORR reaction are due to the chemical adsorption of the O_2 on graphitic BN_3 sites, according to the density functional theory calculations in the study done by Feng *et al.* [33,89].

We used afore ZnO/ZIF-8 basic microparticles as self-sacrifice patterns to create a form of vacuous nitrogen doped carbon microspheres that may be used as powerful electrode materials for ORR activity. Nitrogen doped carbon microspheres received at 1000 ^oC have onset capability, half-wave functionality, and partial modern-day current density of 0.92 V, 0.82 V, and 5.34 mA/cm^2, which is better than nitrogen doped graphitic porous carbon in term of 0.83 V, 0.64 V, and 3.29 mA/cm^2 and Solid carbon spheres that are 0.85 V, 0.72 V, and 3.99 mA/cm^2, which seem to be close to the respective commercial platinum values that are 0.97 V, 0.83 V, and 5.30 m/Acm^2. Our as-organized HNCSs have exhibited exceptional ORR capabilities which are similar with formerly suggested MOF derived heteroatom-doped carbon substances illustrated in **Table 5** [97].

Table 5. ORR efficiency and activity of MOFs derived heteroatom-doped carbon material

Catalysts	Current density (mA/cm^2)	Onset voltage (V)	Halfwave Potential(V)
NGPCs	3.29	0.85	0.72
SCSs	3.99	0.97	0.83
HNCSs	5.34	0.92	0.82
Pt/C	5.30	0.97	0.83

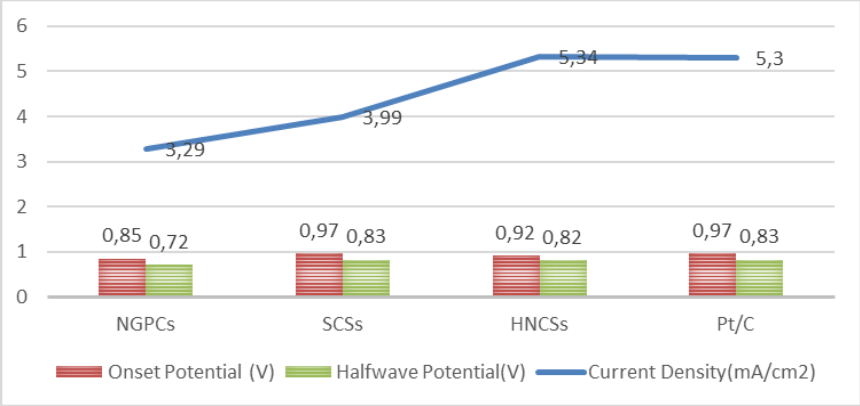

Figure 25. ORR efficiency and activity of MOFs derived heteroatom-doped carbon material

We suggested an innovative, financially viable method to boost ORR catalytic activity by utilizing two homomorphic metal organic frameworks (a) FJU-40-Hand (b) FJU-40-NH_2 to create a fundamental true core MOF-MOF that could regard nitrogen loading and high surface area to obtain a nitrogen doped porous nanocarbon material via a single heat processing in inert atmosphere (**Figure 26**). The time it takes to oxidize carbon is an important factor in ORR efficiency. Nitrogen doped porous carbon b/a-4h appears to have an outstanding ORR performance due to its high surface to volume ratio and high nitrogen loading. Nitrogen doped porous carbon made up of fundamental MOF/MOF has been found to have superior ORR electrocatalytic efficiency than single MOF. Nitrogen doped porous carbon- b/a-4h (-0.068V) > nitrogen doped porous carbon-a/b-4h (-0.075 V) > nitrogen doped porous carbon-a-4h (-0.109 V) > Nitrogen doped porous carbon-b-4h (-0.109 V) > Nitrogen doped porous carbon-b-4h (-0.109 V) (-0.109 V). Furthermore, nitrogen doped porous carbon-b/a (n=4.15) beats nitrogen doped porous carbon-a/b (n=3.32), implying that the nitrogen concentration of receptors interior and exterior core has an impact on ORR capabilities [98].

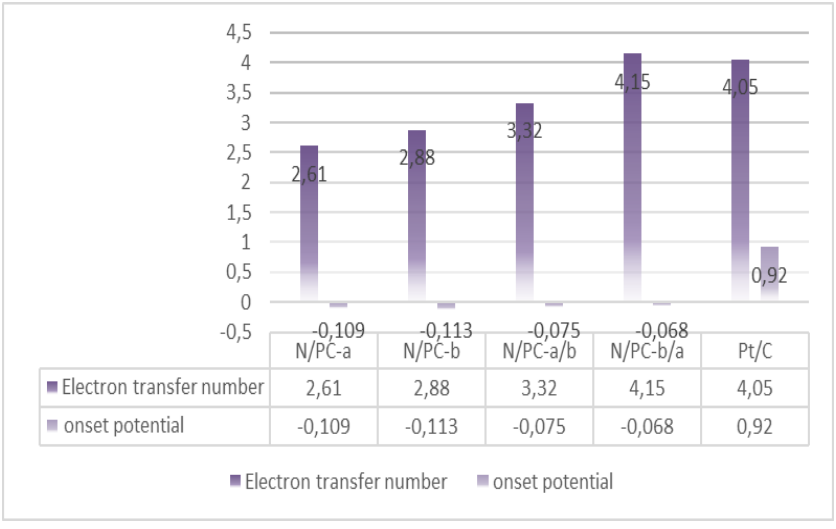

Figure 26. ORR activity of isomorphic MOFs

This study highlighted the preparation of a cobalt@zeolite imidazole framework-8 for Oxygen reduction catalyzed reaction by using tellurium-derived dense carbon nanotubes. For cobalt-containing samples, a suitable quantity of zinc nitrate was substituted with cobalt nitrate, typically between 5 and 100% [85].

Precious metals like platinum and palladium have long been regarded as cutting-edge ORR electrocatalysts. A logical pairing of precious-metal-containing catalysts and Metal organic frameworks can form precious-metal-based ORR electrocatalysts with extraordinary capacity utilization efficiency and strong electrostatic attraction with the carbon substrate. Precious metal-containing precursors can be injected into the porous structure of MOFs just before thermal treatment, and then fused with the carbon materials generated by MOFs. Previously, an employed to fabricate Pt_3Co intermetallic nanomaterials for electrocatalysis on ZIF-8-based carbon was developed. As a precursor, ZIF-8 with 40% Co-doping was used to make nitrogen and cobalt codoped carbon layers (40% Co-N/C). Pt micro particles were then implanted on the carbon layers, which was then autoclaved at 900°C to generate Pt_3Co nanostructures on the carbon substrate that is Pt/40Co-NC-900. In 0.1M $HClO_4$ electrolyte, with an E1/2 capability of 0.92 V, the ORR efficiency of this hierarchical Pt_3Co intermetallic structure outperformed the marketing Pt/C catalyst. By employing a heteroatom-doped carbon matrix to proficiently stabilize valuable metal nanoparticles and non-precious catalysts to regulate the ORR activity, MOFs primarily based on carbon matrix with precious-metal-based binding sites can enjoy the benefits of precious-metal catalysts and gain greater ORR activity and efficiency than promotional valuable metal electrocatalysts [99, 100].

16. Carbon- Based Material

Despite the fact that Pt-based or non-valuable metals catalysts have been established as ORR replacement electrocatalysts, they have a number of drawbacks, including low power density in power devices, selectivity to fuel crossing, and a potentially dangerous nature. The ORR is involved in a wide range of power-related activities, such as energy unit innovation and metal air battery packs, as well as erosion and science [101]. With the rapid advancements in carbon-supported nanostructured materials, a vast number of carbon-supported-metal-free electrocatalysts have been developed that have the ORR catalytic efficiency equal or higher than that of the platinum catalyst and improved stability and fuel tolerance [102-104]. There has been a huge interest in the ongoing search for metal-free ORR electrocatalysts (**Figure 27**) [103].

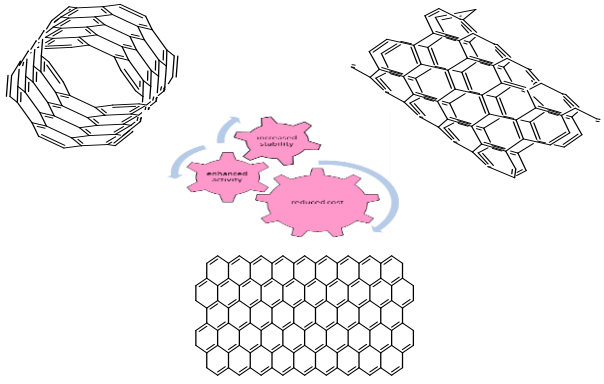

Figure 27. Graphene and CNTs based metal free carbon materials

Carbon-based catalysts such as enacted carbon, carbon fibers, graphene sheets, activated charcoal, carbon nano-tubes, and hierarchical permeable carbon are frequently used in the absence of metal catalysts. With the advancement in changing inherent properties of such carbon-derived materials with a succession of heteroatoms, including boron, nitrogen,

sulfur, selenium, phosphorous, and fluorine, a number of functionalized carbon based impetuses, including a dual functionalized and trio functionalized carbon derived material, have been arranged (**Figure 28**) [14,105]. ORR catalysts have been reported using carbon nanotube, graphene sheets, carbon dots, carbon nanowires, carbon enclosures, and carbons based metal organic frameworks [74,106].

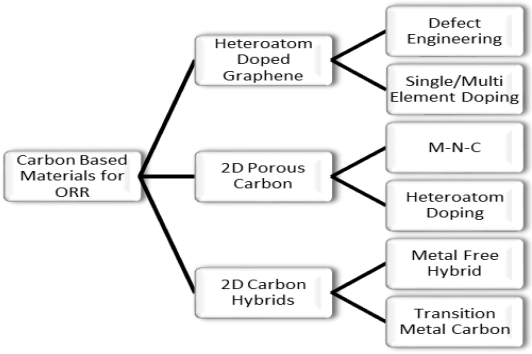

Figure 28. Different carbon based materials

Carbonaceous materials are appealing alternatives to costly PGM-based catalysts due to their abundant resources and high ORR performance. In addition to strong ORR performance in basic medium, some carbon-based electrocatalysts now have competing efficiency, durability, and long run stability in acid conditions. The most common nitrogen bonding arrangements are depicted schematically in **Figure 29** [17].

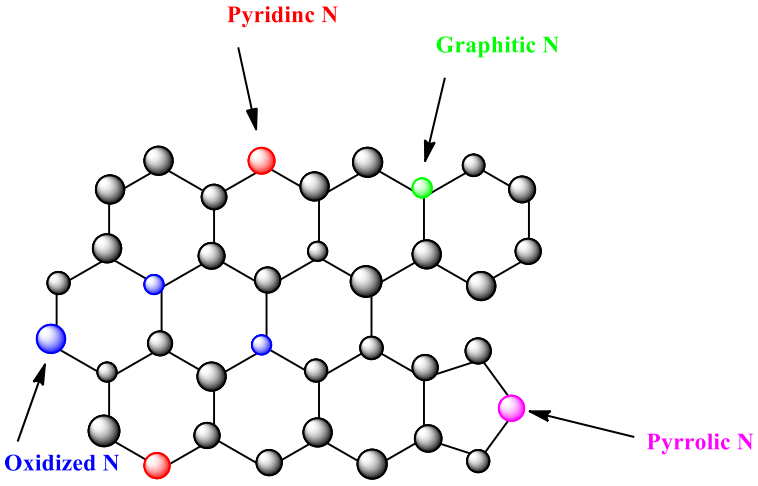

Figure 29. Different types of *N*-bonding arrangement

Another important aspect of nitrogen-alloying into carbon is monitoring the N conformations that are commonly available in many forms, such as pyrrolic-nitrogen, pyridinic-nitrogen, graphitic-nitrogen, oxidized-nitrogen, and the newly found *sp*-hybridized Nitrogen (**Figure 31**). In *N*-alloyed carbons, various conformation coexist, making it difficult to determine which one contributes to the ORR [30]. The synthesis of nitrogen-doped graphene nanostructures was precisely regulated by heat treatment and choosing the appropriate nitrogen precursors, and the findings show that graphite based nitrogen increases the limiting current density, while pyridine-based nitrogen decreases the overvoltage. In situ thermal decomposition of PANi NTs at varying temperatures was also described, resulting in a set of nitrogen dopants on carbon-nanotubes with regulated *N*-conformation. They revealed specimen with the

greatest proportion of graphite based nitrogen and pyridine-based nitrogen has the highest ORR efficiency [14, 90, 107, 108, 109].

Another carbon-based material with the exceptional ORR activity and excellent selectivity, coordinated nitrogen-containing CNTs was reported in 2009, and active areas in *N*-doped carbon have been extensively studied. *N*-doped CNTs as an efficient ORR catalysts with activity 3 times greater than commercial Pt/C in 2009 was described [110]. It is worth noting that introducing a heteroatom which has high electronegativity than carbon, carbon-supported ORR electrocatalyst seems to be an attractive tool for enhancing efficiency, especially when Nitrogen is used. On the other hand, fewer electronegative heteroatoms have been proposed as a viable method of increasing the catalytic performance of these materials. Because of its similar atomic size and electrical structure, nitrogen is perhaps the most successful hetero-atom. This indicates that adding nitrogen to the carbon matrix generates stable species, which is an important factor in producing stable active sites. Other heteroatoms, such as phosphorus or boron, can form stable species with nitrogen. Despite the fact that altering the nitrogen-doped arrangement in carbon-based materials has greatly increased ORR activity, the discovery of active areas, particularly in acidic conditions, remains a pressing need. The inclusion of nitrogen to the sp_2 atomic plane of carbon can alter charge and spin distributions, as well as facilitate the formation of defects. As a result, the individual's internal activity of non-precious metal free carbon-derived composites is significantly lower than that of Pt-based materials. Expanding the numerous accessible effective sites by expanding their contact area is a good way to improve total ORR activity and stability. Porous structure construction is also an excellent way to increase specific electrochemical surface area, and various templates have been investigated for hollow structured materials, including SiO_2, polystyrenes, surfactants, and block copolymers [111].

In the presence of phytic acid, thermal decomposition of polyaniline aerogels yielded microporous carbon nanostructured carbon foams with codopant nitrogen and phosphorous having the bi-functional electrocatalytic activity and efficiency in the Redox reactions like ORR and OER. As the air electrode in metal-air batteries, these metal-free bifunctional catalysts have a lot of potential. For this study, we made two dimensional nitrogen and Sulphur co-doped graphene sheets with an innovative ordered structure made up of 3-dimensional holes on the graphitic surface. SHG has a larger volume, surface area, and more interfacial binding sites for electrochemical processes due to the 3D holes. Because of its historic design with a high specific surface area, rich binding sites, and good electrolyte charge transfer properties, SHG has been shown to be an efficacious tri-functional oxygen reduction response, oxygen evolution response, and hydrogen evolution response catalyst with excellent performance and consistency, outperforming its equivalents without opened gaps or continuous 2-dimensional structure, and so many other carbon-based materials. The SHG is a feasible alternative to worthy metal-based catalysts for energy storage devices including fuel cells, metal–air cells, water splitting, and a wide range of other application domains. The SHG catalyst had a similar onset voltage of 1.01 V, a limited current density of 5.10 mA/cm^2, and a half-wave voltage of 0.87 V to the platinum catalyst, indicating that the two catalysts had similar activities [104].

The phosphorus atom has the same valence electron configuration as nitrogen, but it has a relatively low electronegativity than nitrogen and Carbon. Furthermore, the 3d orbitals can be used to bind this element. Phosphorus doping in carbon materials has received a lot of attention because it suppresses the carbon-oxygen interaction, which is crucial for oxidation and fire resistance. Finding on phosphorus alloyed carbon catalyst is not quite as common in ORR catalysis as it is with nitrogen because the increase in catalytic efficiency is not quite as considerable [19, 89, 90]. The formulation of phosphorus-doped carbon materials and their evaluation for ORR was previously reported. The *p*-doped carbon was created by carbonizing toluene and triphenylphosphine at 1000 ^oC.

Phosphorous-doped carbon nanotubes and virgin carbon nanotubes were compared (CNT). P-CNT had a higher ORR mass activity and higher kinetic current density and onset potential than carbon nanotubes. The improved electrocatalytic efficiency of Phosphorous-doped hierarchical mesoporous carbon was due to covalent bonding of Phosphorous atoms in the carbon network [19, 89, 90, 112, 113]. Previously, carbonization of P-containing PANi, which is acquired by polymerization method in the presence of phytic acid, was regarded as a process for preparing 3D micro porous carbon materials with N and P functional groups. Not only the developed catalyst has a good catalytic activity for ORR, but it also has outstanding catalytic activity for OER. Boron-doped carbon compounds are another form of doped material that might be a potential option for carbon support metal free catalysts. Boron, the same as phosphorus atoms, has a lower electronegativity than nitrogen and carbon atoms, it has been used extensively to suppress CeO_2 reactions. In some experiments, B-doped carbon substances were shown to have an ORR catalytic efficiency similar to commercial platinum nanoparticle catalysts. The enhanced electrocatalytic efficiency of such carbon-supported catalysts is linked to the electron-deficient nature of B-atoms. It has been reported that B and N- co-doped carbon compounds have excellent electrocatalytic performance, even better than platinum commercial catalysts. Sulphides containing 2-carbon atoms and thiols containing 3-carbon atoms are two types of sulphur capabilities that can be observed on the superficial of the carbon catalyst and are classified according to the number of carbons they contain. There are also disulfides to be discovered. Thiols and sulfoxides are the most prevalent *S*-functionalities. Because of the intriguing characteristics generated by the sulphur atoms, sulphur doping in carbon materials has gotten a lot of attention. Previously, reduced graphite oxide doped with sulphur (RGOS) was studied thoroughly. Sulphur atoms were added to the reduced graphite oxide by heating it at 800 ^oC in 1000 ppm hydrogen sulphide in a N_2 atmosphere to produce sulfur-loaded reduced graphite oxide. The inclusion of both sulphur and oxygen atoms in the RGOS is associated with its outstanding performance, and the scientists claim that a comparable atomic quantity is best for optimizing the synergistic effects on ORR [19, 89, 90, 112-114].

Biomass-derived carbon nanotubes have sparked a lot of interest and have been advocated for practice in catalytic applications because of their low cost, renewable nature, and environmental friendliness. Biomass-derived carbon compounds are frequently utilized as the ORR catalysts, either directly or doped with transition metals like Fe, Co, and the novel carbon materials, however these materials are only applicable in an alkaline environment (**Figure 30**). It was reported that hydrothermal treatment of Typha orientalis fower spikes followed by high-temperature annealing in an NH_3 environment to produce nanostructured carbon nanosheets with nitrogen dopant. Carbon nanostructures have a three-dimensional interconnected network structure having high concentration of pyridine and pyrrolic-like nitrogen, and wide surface area with numerous micropores, the produced catalyst worked effectively in an acid medium and a basic medium. As an alternative to metal-based electrocatalyst, effective biomass based carbon has a lot of promise as an oxygen reduction catalyst (ORR). For the first time, enteromorpha based biofuels with nitrogen and sulphur integrated graphene-like framework attached is used as a powerful metal free electrocatalyst for ORR activity. The developed catalyst, which had a low concentration of nitrogen (3.80%), sulphur (1.00%), and a high electrochemical surface area of 778.2 $m2g^{-1}$, had a beginning voltage of 0.95 V against reversible hydrogen electrode in a $4e^-$ route, current density of 4.20mA/cm^2, and demonstrated improved constancy and reliability when matched to marketing platinum catalysts [115].

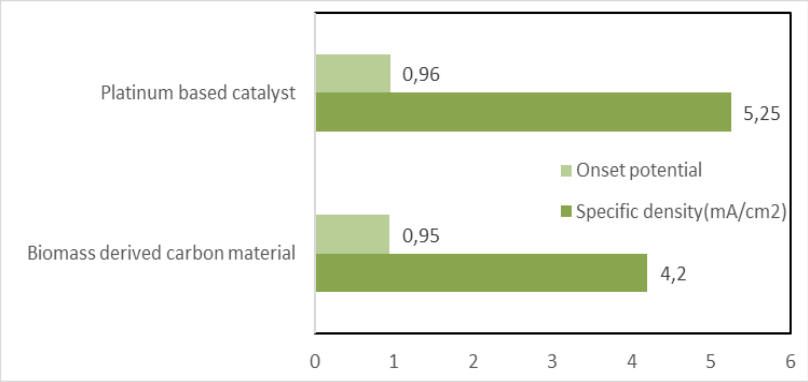

Figure 30. ORR Activity of Biomass carbon materials compared with Pt/C

As in the NH_3 presence, we present a simple and efficient solvothermal technique for producing amino-graphene from graphene oxide. The resulting product, which contains a large number of amino species, can be used as a non-metal ORR electrocatalyst with improved catalytic performance because it has a high nitrogen content of 10.6 % per particle. According to our findings, increasing the kinetic current density in the electrochemical properties for ORR is dependent on the overall amount of graphitic and pyridinic nitrogen atoms. Non-metal ORR electrocatalysts focused on newly discovered amino graphene based compounds with higher nitrogen content, sustainable crystal structure, and convenient method of manufacturing. Because of its semi conductive nature, which prevents transfer of electrons, amino graphene has received little devotion as a multifunctional metal free catalyst for use in alkaline fuel cell technology and other electrochemical processes. It was discovered that G-C_3N_4 has a higher ORR voltage than other Nitrogen-carbons due to the increased nitrogen content in G-C_3N_4, which results in a greater number of binding sites. The current density obtained on sheer G-C_3N_4 declined sharply despite of having higher catalytic activity than sheer carbon because of the catalyst's reduced surface to volume ratio. The ORR performance was significantly better because of a greater proportion of catalytic effective nitrogen groups on the exterior surface of a hierarchical mesoporous G-C3N4 cast with the help of silica nanoparticles SBA-15 as a sacrificial framework. Mixing G-C3N4 with a charcoal having large specific surface area can improve ORR performance and, more importantly, make the 4e reduction reaction easier [116]. Graphene is co-doped with iodine and nitrogen. It is used as a non-metallic motivator for the ORR in both antacid and acidic conditions. The as-synthesized impetus has a strong performance in the alkaline conditions and a beginning voltage of 0.95V, which is nearly comparable to that of ordinary platinum impetus. Plain-Graphene (G), Iodine-Graphene (IG), and Nitrogen-Graphene (NG) have Tafel slopes of 109 $mVdec^{-1}$, 92 $mVdec^{-1}$, and 78 $mVdec^{-1}$, respectively (**Figure 31**). The Tafel slope of the Iodine-Nitrogen-Graphene (ING) is 83 $mVdec^{-1}$, which is similar to the conventional Platinum catalyst, implying that the ORR rate of the iodine and nitrogen co-doped graphene and commercial platinum are the same. The electron-transfer number (n) values for plain graphene, Iodine-Graphene, Nitrogen-Graphene, Iodine Nitrogen co-doped Graphene, and commercial platinum are 3.26, 3.16, 4.13, 4.51, and 4.47, respectively. The fact that the n values of ING and Pt/C are similar suggests that the ORR on ING uses the identical 4e- pathway as commercial platinum [117].

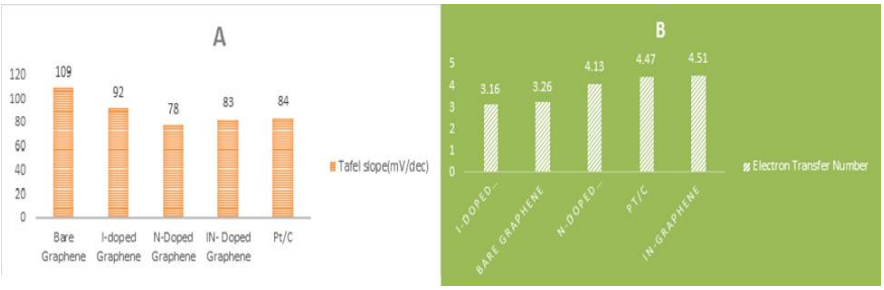

Figure 31. Tafel slope and electron transfer number of different carbon-based material is shown in A and B

Polypyrole nanostructures were activated with potassium hydroxide and heated up to produce porous nitrogen co-doped with carbon nanotubes. Nitrogen doped-CNTs have an active surface area of roughly 1000 $m^2 g^{-1}$, and N-CNT electrode materials, particularly those heated at 900 ^oC, demonstrated good ORR electrocatalytic performance and efficiency, as depicted in **Table 6**. They devised a far more advantageous onset power output better frequency, and longer working consistency in basic conditions when contrasted to a conventionally available 20 wt% Platinum catalyst. The highly permeable tube structures and the synergetic impact among the foremost pyridinic/graphitic-Nitrogen species are fully accountable for this. The N-CNT electrocatalyst performed well in the OER. *N*-CNT-900 was also highly durable and resistant to methanol tolerance and CO intoxication. An alumina template method is used to create almost non-metal, arrayed nitrogen-doped carbon nanotubes, which have a minimal overvoltage and strong ORR response in antacid electrolyte conditions. The kinetic currents for nitrogen-doped-CNT and platinum at 0.1V determined from bends captured at rev/min are 0.91 mA/cm^2 for nitrogen-doped-carbon nanotubes and 0.95mA/cm^2 for conventional platinum. At 0.7V, value of current densities are 11 and 38 mA/cm^2 attained by using N-doped-CNT and commercial Pt electrodes, respectively. Basic anion exchange membrane fuel cells by using N-CNT and commercial platinum as cathodes had the highest power densities of 37.3 and 61.7 mW/cm^2, respectively. The power density of N-CNT & other carbon based materials are given in Table 7. The use of N-CNT as a metal free electrocatalyst is examined for cathodic ORR in MFCs proven effective, with greater electrocatalytic performance, consistency, and dependability than the traditional Pt-impetus. Nitrogen-doped-CNTs appear to be a viable alternative to traditional Platinum electrocatalyst for molten fuel cells, while N-CNT stacking could be enhanced (**Figure 32**) [105-108, 118].

Table 6. ORR activity of N-doped CNT

Catalyst	Reduction Current density(mA/cm^2)	Cathodic Reduction Potential (SCE)	Electron Transfer Number
N-CNT-800	-2.23	-0.181	3.97
N-CNT-900	-2.39	-0.137	3.98
N-CNT-1000	-2.33	-0.136	3.93
Pt/C	-0.93	-0.14	3.71

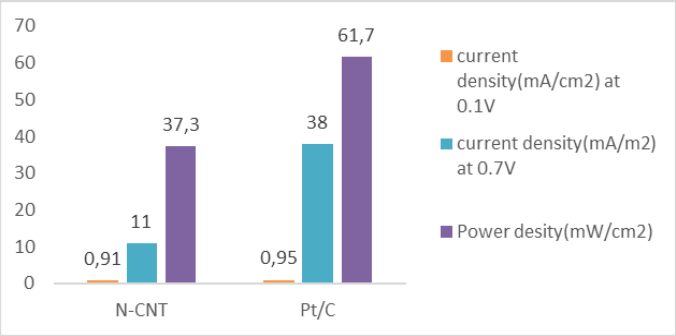

Figure 32. Comparison of ORR activity between N-doped CNT and Pt/C

Carbon nanotubes were ball-milled with thiourea pursued by carbonization, can also produce NS-CNTs with improved ORR performance. Sulfur and nitrogen were incorporated into CNT defect sites. Co-doping with Sulphur can boost the number of nitrogen immersed into the carbon–carbon network which results in collapsing of the carbon-Nanotube structure. The ORR performance of nitrogen-Sulphur-CNTs increases as the heteroatom concentration increases in both antacid and acidic environment. As a result, co-doping with sulfur and nitrogen resulted in more effective electrocatalysts for ORR in acidic environment, because sulphur stimulates the incorporation on nitrogen surface. Vertically aligned CNTs were initially employed as an improved carbon nanomaterial support for co-doping to achieve the higher ORR activity. On the SiO_2/Si surface, decomposition of melamine diborate produced erect stacked boron and nitrogen co-doped carbon nanotubes with fairly similar lengths of B15 millimeter. In erratically stacked boron and nitrogen co-doped carbon nanotubes contains the carbon content (85.5%) surpasses chemically coupled with boron (4.2%) and nitrogen (4.2%). The high carbon content of vertically stacked BN-CNTs provides good conductance for electrocatalysis purposes, while the alloying elements boron and nitrogen considerably boost ORR activity. The fact that ORR performance decreases as the B/N ratio increases in B-N-CNTs indicates that bonded boron and nitrogen have only a limited role in ORR performance. From the other hand, increasing the B/N ratio can boost the ORR catalytic capacity of B-CNTs-N [119, 120].

Table 7. ORR performance of different carbon based materials

Catalysts	Catalyst Loading(mg/cm$^{2)}$	Power Density(mW/cm^2)
Fe,Co/NC	0.77	980
Fe/N/C-SCN	4	1030
Fe/Phen/Z8	4	910
Fe-doped Zn ZIF-8	4.5	820
CNT/PC	3.05	379
Fe/N/CF	3	900
PANI-FeCo-C	4	550
SA-Fe/NG	N.A	823
Co-N-C	4	870
Co-FeN_X	6	520
N-CNT	N.A	37.3

17. Single Atom-Based ORR Catalyst

In the domain of oxygen reduction cathode materials research, single atom-based catalysis in which metal binding sites are scattered at the atomic level is an intensively studied. SACs are thought to hold a lot of promise for reducing PGM consumption because of their high atomic

radii and unique properties. SACs are a new addition to the large group of ORR electrode material that are platinum group metal, non-platinum group metal, and carbon derived materials. They are also comprehensive example, which could enhance the efficiency among all varieties of catalysts. Transition metal single-atom catalysts (SAC) have sparked a lot of interest on the ORR cathode as a replacement for Platinum catalysts [121]. Despite the fact that Cupper is the natural choice for ORR electrocatalyts in a range of species, from *bacillus* species to humans, several analyses of Cu-based SAC for ORR electrocatalytic reaction have been conducted. The cupper based SAC was made using Cupper phthalocyanine as a precursor and a simple carbonization method. The ORR process conducted in basic medium, the catalyst has an $E_{1/2}$ voltage of 0.81 V against reversible hydrogen electrode. An AEM fuel cell is a sort of energy component that utilizes Cu-based single atom catalyst and has a most extreme power thickness of 196 $mWcm^{-2}$ at 70 °C. According to the DFT computation, the rate limiting step over Copper based single atom catalyst, is the transformation from OOH* to O*. The Cu-based single atom catalyst has potency to be a viable non-valuable oxygen reduction electrode material for electrochemical devices like fuel cells [122].

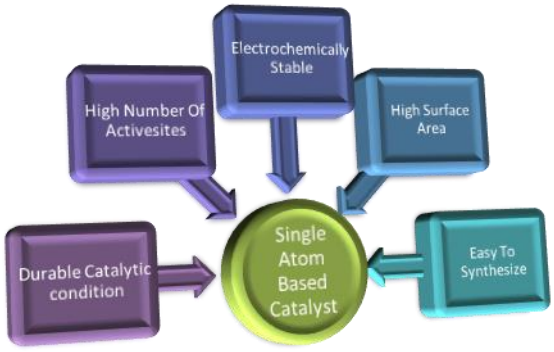

Figure 33. Properties of single atom based electrocatalysts for ORR process

Single atom electrocatalysts have the power to enhance ORR catalytic reaction pricing, efficiency, and reliability by merging the robustness of homogeneous and heterogeneous electrocatalysts (**Figure 33**). Significant progress is required due to the lack of high-activity, single atom-based catalysts and one's precise catalytic reactions. Foremost, we reported iridium-based single atom catalyst for ORR catalytic process with maximum reliability and performance that looks like homogeneous iridium porphyrins. With a solid turnover recurrence of $24.3e^{-1}site^{-1}s^{-1}$ at 0.85 V against reversible hydrogen electrode and an outstanding ORR activity of 12.2 A/mg, the as-synthesized Ir-based-SAC shows more prominent ORR execution in orders of magnitudes than Iridium based nanoparticles. The cathode of Iridium single atom cell had a higher electric potential of 0.955 V, which is nearly identical to the Platinum cathode cell. The fuel cell's highest power density was 932 mW/cm^2, which is higher than other non-platinum ORR catalysts, demonstrating Ir-significant SAC's promise as a high-efficiency alternative to precious metal catalysts in fuel cell technology [123].

The spectroscopic assurance of the coordination construction of the molecularly dissipated CuNx spots and its effect on ORR activity in Cu-N-C impetuses was recently revealed. With adjustable geometric shapes incorporated in nitrogen-doped graphene lattices, a logical method for accessing the atomically scattered CuNx molecules was presented. An original blend technique involving the use of thiourea as an "in situ decreasing specialist" was described to change the binding sites of single cupper particles [124]. Cu-based single atom catalyst which is molecularly

scattered Cu moored on N-doped graphene, was first made by using a two-steps pyrolysis strategy that included CuPc and dicyandiamide. Thiourea was used as an in situ reducing specialist in order to create a CuI N_2-rich specimen, and it was applied at the same temperature (Cu-NGS). Copper moored with N-doped graphene and Cupper attached with N-doped grapheme and thiourea stacking substances were nearly indistinguishable. The related evaluations showed that increasing CuI-N_2 levels increases ORR activity, proving that thiourea based Cu-SAC is the true effective site for ORR at cathode. Cu-NGS has a significantly higher kinetic current density value 15.36mA/cm^2 than Cu-NG, indicating rapid reaction kinetics and greater intrinsic electrocatalytic activity [122, 125].

Another single-molecule scattered cobalt site with non-planar collaboration has been succeeded in making nitrogen supported on carbon. After this doping, the ORR execution and effectiveness of impetuses are surveyed and examined. With a high starting voltage of 0.96, 0.01 V and an $E_{1/2}$ potential of 0.85, 0.01 V, this device has a lot of potential. The action of Co-N-C-700 is ominously advanced than that of Co-N-C-700 without cobalt impetuses. When compared with conventional 20% Platinum catalyst these qualities appear to be 0.2 V higher than those of carbon-supported planar cobalt with beginning capabilities of 0.97 and 0.85V. Furthermore, the Tafel slope of cobalt-SAC-700 was 78 mV/dec1, slightly higher than that of platinum impetus, which was 73 mV/dec1 (**Figure 35**) [126, 127].

Single-atom FeSACs catalysts, in which FeN4 moieties created by coordination of single-atom Fe with nitrogen are considered as the active sites for ORR can maximize metal site utilization while accelerating catalytic efficiency. The comparison of different reported electrocatalysts are illustrated in Table 8. As a result, significant Fe loading in single-atom motivators is challenging to attain, resulting in poor performance. The Fe_{AC}/ Fe_{SAN}-C materials excellent performance is even further proven by the strong 'J_k' active current density at 0.85 V is 61.1 mA/cm^2, that demonstrates the Fe_{AC}/ Fe_{SAN}-C catalyst's greater efficiency with an $E_{1/2}$ value of 0.912 V, which is significantly greater than that of conventional platinum catalyst at 0.897 V and the majority of reported Fe-based single atom catalysts [15].

A Ru-NC catalyst for increased performance of ORR catalysis by using micro porous metal organic frameworks (MOFs) restricted approach. A metalorganic framework (MOF)-assisted host guest approach was used to produce Ruthenium single site with mesoporous zeolite imidazolate frameworks-8 as the host guest. Ru-SSC has significantly better stability than Fe-SSC that is after 20000 loops, there was only a 17 mV negative shift. Ru-high SSC's activity and stability in a true fuel cell system supports its practical application. Owing to their high atom utilization, the single-atom electrocatalysts have been hailed as one of the most favorable catalysts for ORR. The use of atomically dispersed platinum atoms on zeolite-supported carbon to achieve a high platinum loading of 5%. By using a two-electron route rather than the traditional four-electron method, this catalyst produced H_2O_2 with excellent selectivity. For ORR in acidic medium, the as-acquired impetus has a beginning voltage of 0.71 V versus RHE. 6.7 wt% adjacent distributed Pt atom supported on ultrathin Fe-Pt nanosheets was also synthesized. The systematic activity of the single atom catalyst as prepared is 0.566 A/mg$_{Pt}^1$ that is roughly 7 fold higher than that of traditional platinum for ORR with excellent CO tolerance. Another multifunctional catalyst Pt_1/ATO with up to 8% single atomic Pt loading. For ORR, the as-prepared catalyst demonstrated good activity and durability [128].

We used MOFs as a settling grid for the first time to foster carbon-based chromium single particle impetus for the ORR, in which the atomic design scattered chromium, is checked to have a Cr-N4 collaboration structure. With an ideal half wave voltage of 0.773 V against RHE, the Cr-N supported on carbon impetus has a decent oxygen reduction movement. In the chromium-SAC union technique, the ZIF-8 skeleton assimilates hydrolyzed $CrCl_3$ into its porous structure via host-guest communications. The absence of a Cr-N dispersing course indicates that chromium

atoms were restricted in the small pores rather than subbing the zinc hubs in the edge. A complex pyrolyzed Cr-SACs framework catalyzed the acidic ORR, which performed admirably [129].

We propose a surfactant-assisted method for creating iron based single atom impetuses in this review. In acidic conditions, the half wave voltage of single particle based iron impetus is only 30 mV lower than conventional platinum impetus, though it is 30 mV more prominent in essential conditions. Single atom-Fe/NG is also extremely stable, with just 12 mV and 15 mV negative movements after 5000 circles, in both alkaline and acidic conditions. The peak power thickness of the fermented proton exchange membrane energy component, which is dependent on Fe-based single atom, is unimaginable at 823 mW/cm^2 (**Figure 34**) [130]. As previously mentioned, SACs have a great deal of promise for use in proton exchange membrane power modules and metal air batteries. By definitively directing the planning environmental elements and expanding the construction penetrability and surface space of the limiting locales, SACs' inborn synergist movement can be further tuned and improved. However, MEA by using single atom catalyst as counter electrode catalysts has reduced energy and peak power densities than Precious metal catalysts. Furthermore, because separated atoms have a large surface area, most widely available single atom catalyst have a low utilization quantity usually less than 1 % wt to prevent accumulation and recrystallization, limiting the overall number of binding sites that can be found in single atom catalysis. Moreover, most SAC production methods are complex and time-consuming, making large-scale manufacturing of good-quality SACs a major problem at the moment [131].

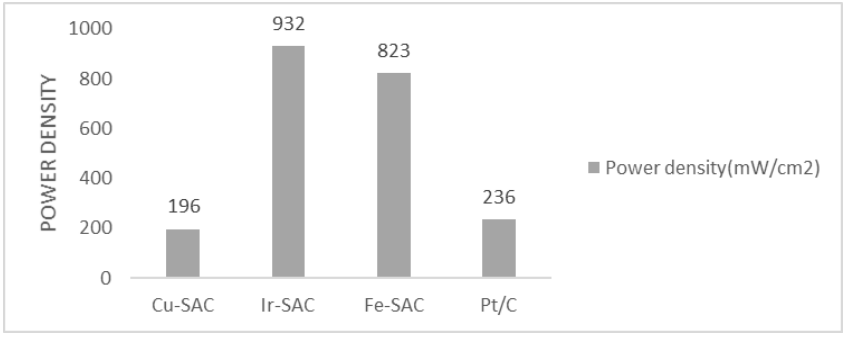

Figure 34. Power density shown by different single atom based catalysts

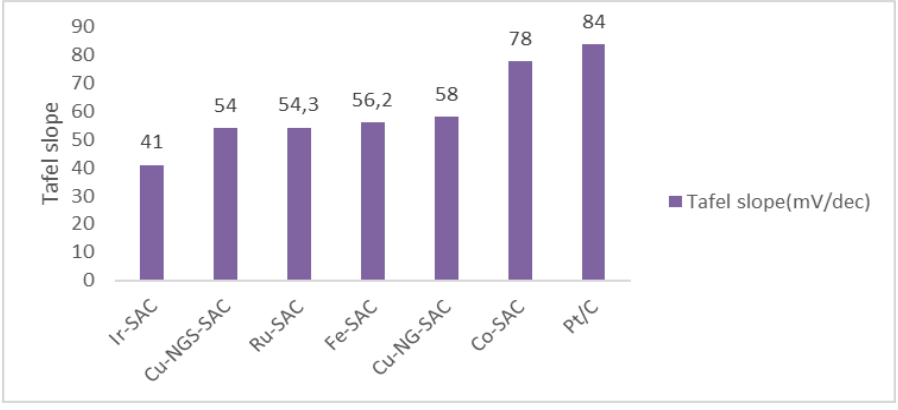

Figure 35. Tafel slope of different single atom based catalyst compared with Pt/C

Table 8. ORR activity of different reported electrocatalysts

Catalyst	Onset Potential	Current Density (mA/cm^2)	Power Density(W/cm^2)
Fe-Co-N/C	0.7	500	0.98
Ti-Co-N	0.7	38	0.108
Mn-N/C	0.7	350	0.46
Fe-N/C	0.7	637	0.75
Co-N/C	0.7	250	0.56
Pt-Co/C	0.7	720	0.65
L_{10}Pt-Co	0.7	800	N.A
Pt-Co/C	0.7	1500	1.42
PtNi	0.7	1130	0.92
Pt/C	0.9	530	23.6
Ir-SAC	0.95	N.A	93.2
Cu-SAC	0.85	N.A	19.6
Fe-SAC	0.9	4.7	82.3
ZIF-750	0.90	12.22	N.A
ZIF-ppy/PANI	0.93	24.94	N.A
Co@NPC	1.39	5.3	7.875
FCPA-800	0.84	4.80	N.A
FCPA-900	0.87	5.68	N.A
FCPA-1000	0.88	4.34	N.A
Fe_3Mn1/NCNTs-100	0.86	1.447	N.A

18. Conclusion

Among the recent theoretical advances in energy conversion technology and energy storage devices, platinum free catalyst and non-precious metal catalysts incredibly stable and limited-cost. The main obstacles for developing premium, effective, and stable catalysts are: (i) consistency, (ii) inventive definition strategies and extensive characterization of the electrochemical intersections, and (iii) nano-underlying mixing, alongside their controllable extents. The core problem with fuel cell technology is the slow ORR at cathode. As a result, fine-tuning experiments are essential for learning more about heterogeneous catalysis of electrochemical reactions including oxidation reduction and how it varies from catalyst science. The electronic properties of binding sites was successfully changed engineering nanomaterials and adjustable composition, resulting in a significant increase in performance and efficiency. For related devices and power conversion technologies, it is important to investigate low-cost ORR electrocatalysts with high efficiency, stability, and reliability. The enormous voltage of ORR electrocatalyst for energy storage devices was demonstrated in this study. To achieve better catalytic performance and stability, the layout of a new ORR oxygen reduction electrocatalyst is inextricably connected to the concept of either a new platinum catalyst or platinum-free catalysts. The current search for improved catalysts has resulted in some interesting breakthroughs in our knowledge of catalysis, enabling for more rational manipulation of catalytic characteristics through controlled synthesis. By adjusting the exposed aspects or doping platinum with other transition metals, the surface chemisorption characteristics of platinum catalysts have been rationally manipulated, resulting in highly effective platinum-based catalysts. Controlling the size, compositional profile, and morphology of platinum based catalysts can strengthen their catalytic properties. With the release of the Toyota "Mirai," the first commercially available gasoline vehicle, other multinational corporations started to compete by designing appropriate hydrogen fuel cells. Regardless of the fact that different platinum group metal

derived catalysts such as core platinum polyhedral structures and nanoframes with a high porosity have been created with far more than an approximate amount of greater mass activity by the rotating disk electrode tests. The Toyota Mirai Fuel Cell Vehicle to this day uses platinum-cobalt alloy nanostructures as a catalyst. The far more important task for the growth of linked power generation systems is the progression of cost-effective and long-lasting ORR electrode materials. In the industrial production of catalysts, reliable, and consistent control for different brands is required to maintain stable fuel cell operation. The framework of platinum-based catalysts with curved morphological features appears to be difficult to maintain in mass production, and surface deformation is likely to destroy shape-dependent properties. As a result of their scattering, ductility, and reaction routes, g-carbon matrix should be considered in the interconnected formation of platinum-based catalysts. In the case of non-platinum catalysts, various additional noble metal catalysts like palladium and ruthenium have been investigated as replacements for platinum. Palladium-based catalysts have a larger particle dimension than platinum-based catalysts. Palladium is a good material for significant formic acid fuel cells and basic fuel cells that operate on ethyl alcohol and isopropyl alcohol, but more studies are needed. The growth of effective, moderate-price, and non-noble ORR metal electrocatalyst materials to substitute the as of now used. For the continuing commercialization of PEM fuel cells, platinum catalysts are necessary. Carbon-supported catalysts are the most favorable ORR electrocatalysts among non-precious metal electrocatalysts because they have the ORR efficiency and consistency comparable to conventional available platinum catalysts. Even so, because it entails substituting a more expensive metal catalyst with a low-cost metal with reduced efficiency; these catalysts are only used in a restricted number of applications. Non-noble metal have previously shown significant increases in ORR performance, completely replacing pure noble metals. Carbon-based with nitrogen dopant electrocatalysts, both with and without transition metal participation metal based carbon with nitrogen dopant or nano-carbon, also fascinated interest among the various methods being investigated.

Compared with the plain carbon catalyst, doping of nitrogen in carbon materials is needed for remarkably improved ORR efficiency, irrespective of whether metal atoms take part immediately in binding sites or merely speed up their formation. Although non-metal nitrogen dopant carbons material can provide considerable ORR efficiency, a transition metal is needed to form extremely g-carbon nanomaterials in situ, resulting in more effective and long lasting catalysts. Although these non-platinum catalysts can accelerate the ORR process in an aqueous medium, their specificity and reliability in an acidic medium are low. Theoretical and experimental interpretations of the origins of binding sites and their correlation to electrocatalysts effective surface area and morphology are urgently needed at this time to propose new non platinum noble metal catalysts and ORR performance levels. The ORR performance could be improved by fine-tuning the catalyst formation medium to achieve a high active surface area or active site usage. Although current catalysts are unable to meet the serious hurdles of energy efficient technologies, the investigation and refinement of many nanostructured ORR electrocatalysts including the control of dimensions, form, morphology, framework, and interface engineering, as well as it will be vital to achieve understanding of the nature of catalytic performance and efficiency.

19. Future Perspectives

Scientists in this field are always trying to figure out where ORR catalysts get their maximum catalytic activity. Probing effective binding sites and detailed characterization of effective binding sites are critical for establishing the structure–function link. The high catalytic performance electrocatalysts is mostly determined by their structure. As a result, design approach is a significant area for the introduction of new electro active technologies. This brief study seeks to provide an overview on the state of the art in modern oxygen reduction catalyst research that relies on

carbon, MOFs, and free of noble metals. We anticipate that this research study will offer some valuable information for the forthcoming creation of ORR electrocatalysts.

i. ORR electrode materials have the advantage of just being stable in acidic conditions. A beneficial approach to achieve this target is multi-doping, which exploits customizable doping schemes to create active sites that are instantaneously transferring partial positive carrier. Because so many metal-free substrates have been created by various methods over the recent decades, there is nevertheless a considerable distance to go before oxygen reduction electrocatalysts are commonly used in real world applications.

ii. Classic electrocatalysts can be extended by model electrocatalysts to reveal robust nanostructures. It is vital to use a particular process employing nitrogen-doped carbon nanomaterials that are free of the impacts of basic carbon defects and pathogenic. To build stunning nanomaterials for oxygen reduction reaction in acidic environments, nitrogen-doped electrocatalysts with accurate multi-doping configurations are particularly crucial.

iii. Half-cell studies are a valuable method for the investigation and evaluation of the intrinsic efficiency and oxygen reduction rates of electrode materials. The RDE tests and assessment by using extremely thin films are inadequate because the prime driving variables underlying fuel cell effectiveness, such as ion transport, water, and heat regulation, and mass displacement are absent. Possible improvements in this area are advised to include fuel cell observations and analysis.

iv. For the improvement of efficiency and progress of fuel cell technology, the pattern and strategy of the electrode nano materials are very important. By enabling mass transfer, innovative layout can improve the efficiency of the effective sites. Furthermore, it offers tearing methods and procedures to boost the electrocatalyst's efficiency, which improves fuel cell technology performance.

v. Rarely have electrocatalysts built on MOFs been studied for organic compounds, particularly carbon dioxide reduction. Mesoporous electrocatalysts might effectively compensate electrocatalytic robustness. Furthermore, in acid conditions, the electrochemical activity of metal organic framework based nanostructures should be increased in terms of kinetics and stability. For the power conversion purposes, efficient and reliable metal organic framework based nanocatalysts with certain characteristics are essential.

vi. The main driving force behind single atom oxygen reduction catalytic performance in the coming years is the development of nanostructured materials. The novel nanostructures should surpass the prior obstacles and satisfy the minimum specifications like minimal rates of raw goods and manufacturing process, exceptional oxygen reduction catalytic performance of electrocatalyst for use in industrial applications, durability that appropriately regulates the commercial gadget for a few generations and scalability for mass industrialization. Hence, future studies will need to put in even more work.

vii. Single atom electrode materials require in-depth investigation and analysis. Both mechanical investigations and a comprehensive evaluation of oxygen reduction reaction in an acidic and alkaline electrolytic condition are greatly sought. The creation of single atom based catalyst on a massive scale for industrial usage is a challenging task because the fabrication techniques for multiple kinds of single atom electrocatalyst are labor-intensive. As a result, general conferences that can be amended and enhanced for the simplistic synthesis of a broad range of single atom electrocatalyst are highly required. Because of their unique characteristics and low price, the advancement of single atom

viii. electrocatalysts by using non-noble metals is an excitingly interesting move. Therefore, more in-depth investigational research is needed for non-precious single atom based electrocatalyst that may provide an excellent path that leads for the progress of electrocatalysis in the coming years.

For such study of the non-precious single atom based electrocatalytic process of a single effective site, sophisticated technologies and computational modeling should be applied. Predicting the structure single atom based catalyst by using quantitative parameters of an imaginative manufacturing technique and novel functional catalytic system is vital. Researching active single atom with commendable performance, long-term endurance, and budget requires work. Studying single atom based catalyst with improved characteristics is crucial for catalytic performance and other energy-related applications.

Acknowledgment

We are thankful to the University of Wah, Quaid Avenue, Wah Cantt for providing us research and technical facilities.

Orcid:

Fawad Ahmad
https://www.orcid.org/0000-0003-2404-5572

Khusbo-e-Kainat
https://www.orcid.org/0000-0002-9582-981X

Umer Farooq
https://www.orcid.org/0000-0002-8226-5605

References

[1]. X. Tian, X.F. Lu, B.Y. Xia, X.W.D. Lou, *Joule*, **2020**, *4*, 45-68. [Crossref], [Google Scholar], [Publisher]
[2]. A.G. Olabi,. T. Wilberforce, M.A. Abdelkareem, *Energy*, **2021**, *214*, 118955. [Crossref], [Google Scholar], [Publisher]
[3]. G. Wu, K.L. More, C.M. Johnston, P. Zelenay, *Science*, **2011**, *332*, 443-447. [Crossref], [Google Scholar], [Publisher]
[4]. J. Wu, and H. Yang, *Acc. Chem. Res.*, **2013**, *46*, 1848-1857. [Crossref], [Google Scholar], [Publisher]
[5]. M.D. Bhatt, J.Y. Lee, *Energy Fuels*, **2020**, *34*, 6634-6695. [Crossref], [Google Scholar], [Publisher]
[6]. A.M. Gómez–Marín, E.A. Ticianelli, *Curr. Opin. Electrochem.*, **2018**, *9*, 129-136. [Crossref], [Google Scholar], [Publisher]
[7]. F. Jaouen, E. Proietti, M. Lefèvre, R. Chenitz, J.P. Dodelet, G. Wu, H.T Chung, C.M. Johnston, P. Zelenay, *Energy. Environ. Sci.*, **2011**, *4*, 114-130. [Crossref], [Google Scholar], [Publisher]
[8]. S. Yi, H. Jiang, X. Bao, S. Zou, J. Liao, Z. Zhang, *J. Electroanal. Chem.*, **2019**, *848*, 113279. [Crossref], [Google Scholar], [Publisher]
[9]. F. Jaouen, D. Jones, N. Coutard, V. Artero, P. Strasser, A. Kucernak, *Johnson. Matthey. Technol. Rev.*, **2018**, *62*, 231-255. [Crossref], [Google Scholar], [Publisher]
[10]. Y. Feng, N.A. Vante, *physica. status. solidi.*, **2008**, *245*, 1792-1806. [Crossref], [Google Scholar], [Publisher]
[11]. Z. Chen, D. Higgins, A. Yu, L. Zhang, J. Zhang, *Energy. Environ. Sci.*, **2011**, *4*, 3167-3192. [Crossref], [Google Scholar], [Publisher]
[12]. E. Antolini, *Energy. Environ. Sci.*, **2009**, *2*, 915-931. [Crossref], [Google Scholar], [Publisher]
[13]. H.F. Wang, L. Chen, H. Pang, S. Kaskel, Q. Xu, *Chem. Soc. Rev.*, **2020**, *49*, 1414-1448. [Crossref], [Google Scholar], [Publisher]
[14]. J.Q. Bermejo, E. Morallón, D.C. Amorós, *Carbon*, **2020**, *165*, 434-454. [Crossref], [Google Scholar], [Publisher]
[15]. X. Li, S. Duan, E. Sharman, Y. Zhao, L.Yang, Z. Zhuo, P. Cui, J. Jiang, Y. Luo., *J. Mater. Chem.*, **2020**, *8*, 10193-10198. [Crossref], [Google Scholar], [Publisher]
[16]. J. Zhang, H. Yang, J. Fang, S. Zou, *Nano Lett.*, **2010**, *10*, 638-644. [Crossref], [Google Scholar], [Publisher]
[17]. Y. Nie, L. Li, Z. Wei, *Chem. Soc. Rev.*, **2015**, *44*, 2168-2201. [Crossref], [Google Scholar], [Publisher]
[18]. H. Meng, P.K. Shen, *Electrochem. Commun.*, **2006**, *8*, 588-594. [Crossref], [Google Scholar], [Publisher]
[19]. M.D. Cueto, P. Ocón, J.M.L. Poyato, *J. Phys. Chem. A*, **2015**, *119*, 2004-2009. [Crossref],

[Google Scholar], [Publisher]
[20]. Y. Sha, T.H. Yu, B.V. Merinov, P. Shirvanian, W.A. Goddard, *J. Phys. Chem. A*, **2012**, *116*, 21334-21342. [Crossref], [Google Scholar], [Publisher]
[21]. A. Kulkarni, S. Siahrostami, A. Patel, J.K. Nørskov, *Chem. Rev.*, **2018**, *118*, 2302-2312. [Crossref], [Google Scholar], [Publisher]
[22]. M.V. Kannan, G.G. Kumar, *Biosens. Bioelectron.*, **2016**, *77*, 1208-1220. [Crossref], [Google Scholar], [Publisher]
[23]. A. Wieckowski, Fuel cell catalysis: a surface science approach., **2009**. [Google Scholar], [Publisher]
[24]. J.H. Hirschenhofer, "Fuel cells: a handbook." **1994**. [Google Scholar], [Publisher]
[25]. O.Z Sharaf, M.F. Orhan, *Renew. Sust. Energ. Rev.*, **2014**, *32*, 810-853. [Crossref], [Google Scholar], [Publisher]
[26]. Z. Zhao, C. Chen, Z. Liu, J. Huang, M. Wu, H. Liu, Y. Li, Y. Huang, *Adv. Mater.*, **2019**, *31*, 1808115. [Crossref], [Google Scholar], [Publisher]
[27]. R. Lin, X. Cai, H. Zeng, Z. Yu, *Adv. Mater.*, **2018**, *30*, 1705332. [Crossref], [Google Scholar], [Publisher]
[28]. M. Liu, Z. Zhao, X. Duan, Y. Huang, *Adv. Mater.*, **2019**, *31*, 1802234. [Crossref], [Google Scholar], [Publisher]
[29]. Y.J. Wang, W. Long, L. Wang, R. Yuan, A. Ignaszak, B. Fang, D.P. Wilkinson, *Energy. Environ. Sci.*, **2018**, *11*, 258-275. [Crossref], [Google Scholar], [Publisher]
[30]. J. Zhu, M. Xiao, K. Li, C. Liu, X. Zhao, W. Xing, *ACS Appl. Mater. Interfaces.*, **2016**, *8*, 30066-30071. [Crossref], [Google Scholar], [Publisher]
[31]. H. Lv, D. Li, D. Strmcnik, A.P. Paulikas, N.M. Markovic, V.R. Stamenkovic, *Nano Energy*, **2016**, *29*, 149-165. [Crossref], [Google Scholar], [Publisher]
[32]. C.V. Rao, B. Viswanathan, *J. Phys. Chem. C.*, **2009**, *113*, 18907-18913. [Crossref], [Google Scholar], [Publisher]
[33]. Q. Ren, H. Wang, X.F. Lu, Y.X. Tong, G.R. Li, *Adv. Sci.*, **2018**, *5*, 1700515-1700536. [Crossref], [Google Scholar], [Publisher]
[34]. X.H. Tan, S. Prabhudev, A. Kohandehghan, D. Karpuzov, G.A. Botton, D. Mitlin, *ACS Catal.*, **2015**, *5*, 1513-1524. [Crossref], [Google Scholar], [Publisher]
[35]. N. Wada, M. Nakamura, N. Hoshi, *Electrocatalysis*, **2020**, *11*, 275-281. [Crossref], [Google Scholar], [Publisher]
[36]. M. Shao, *J. Power Sources.*, **2011**, *196*, 2433-2444. [Crossref], [Google Scholar], [Publisher]
[37]. O. Savadogo, K. Lee, k. Oishi, S. Mitsushima, N. Kamiya, K.I. Ota, *Electrochem. commun.*, **2004**, *6*, 105-109. [Crossref], [Google Scholar], [Publisher]
[38]. M. Neergat, V. Gunasekar, R. Rahul, *J. Electroanal. Chem.*, **2011**, *658*, 25-32. [Crossref], [Google Scholar], [Publisher]
[39]. C. Du, X. Gao, W. Chen, *Chinese J. Catal.*, **2016**, *37*, 1049-1061. [Crossref], [Google Scholar], [Publisher]
[40]. M. Nunes, D.M. Fernandes, M.V. Morales, I.R. Ramos, A.G. Ruiz, C. Freire, *Catal. Today.*, **2020**, *357*, 279-290. [Crossref], [Google Scholar], [Publisher]
[41]. A. Holewinski, J.C. Idrobo, S. Linic, *Nat. chem.*, **2014**, *6*, 828-834. [Crossref], [Google Scholar], [Publisher]
[42]. C.L. Lee, H.P. Chiou, C.M. Syu, C.R. Liu, C.C. Yang, C.C. Syu, *Int. J. Hydrog. Energy.*, **2011**, *36*, 12706-12714. [Crossref], [Google Scholar], [Publisher]
[43]. Y. Lu, N. Zhang, L. An, X. Li, D. Xia, *J. Power Sources.*, **2013**, *240*, 606-611. [Crossref], [Google Scholar], [Publisher]
[44]. N. Zhang, X. Chen, Y. Lu, L. An, X. Li, D. Xia, Z. Zhang, J. Li, *Small*, **2014**, *10*, 2662-2669. [Crossref], [Google Scholar], [Publisher]
[45]. L. Kuai, X. Yu, S. Wang, Y. Sang, B. Geng, *Langmuir*, **2012**, *28*, 7168-7173. [Crossref], [Google Scholar], [Publisher]
[46]. R. Zhang, W. Chen, *J. Mater. Chem.*, **2013**, *1*, 11457-11464. [Crossref], [Google Scholar], [Publisher]
[47]. C. Xu, Y. Liu, H. Zhang, H. Geng, *Asian J. Chem.*, **2013**, *8*, 2721-2728. [Crossref], [Google Scholar], [Publisher]
[48]. H. Zhang, Q. Hao, H. Geng, C. Xu, *Int. J. Hydrog. Energy.*, **2013**, *38*, 10029-10038. [Crossref], [Google Scholar], [Publisher]
[49]. Z. Zhang, K.L. More, K. Sun, Z. Wu, W. Li. *Chem. Mater.*, **2013**, *23*, 1570-1577. [Crossref], [Google Scholar], [Publisher]
[50]. G. Jiang, H. Zhu, X. Zhang, B. Shen, L. Wu, S. Zhang, G. Lu, Z. Wu, S. Sun, *ACS Nano.*, **2015**, *9*, 11014-11022. [Crossref], [Google Scholar], [Publisher]

[51].
[52]. L. Chen, H. Guo, T. Fujita, A. Hirata, W. Zhang, A. Inoue, M. Chen, *Adv. Funct. Mater.*, **2011**, *21*, 4364-4370. [Crossref], [Google Scholar], [Publisher]
[53]. Y. Qi, J. Wu, H. Zhang, Y. Jiang, C. Jin, M. Fu, H. Yang, D. Yang, *Nanoscale*, **2014**, *6*, 7012-7018. [Crossref], [Google Scholar], [Publisher]
[54]. D.S. Su, G. Sun, *Angew. Chem. Int. Ed.*, **2011**, *50*, 11570-11572. [Crossref], [Google Scholar], [Publisher]
[55]. H. Nolan, M.P. Browne, *Curr. Opin. Electrochem.*, **2020**, *21*, 55-61. [Crossref], [Google Scholar], [Publisher]
[56]. Z. Lu, H. Wang, D. Kong, K. Yan, P.C. Hsu, G. Zheng, H. Yao, Z. Liang, X. Sun, Y. Cui, *Nat. commun.*, **2014**, *5*, 1-7. [Crossref], [Google Scholar], [Publisher]
[57]. C.W.B. Bezerra, L. Zhang, K. Lee, H. Liu, A. L.B. Marques, E.P. Marques, H. Wang, J. Zhang, *Electrochim. Acta*., **2008**, *53*, 4937-4951. [Crossref], [Google Scholar], [Publisher]
[58]. C. Domínguez, F.J. Pérez-Alonso, M. Abdel Salam, J.L.G. De La Fuente, S.A. Al-Thabaiti, S.N. Basahel, M.A. Peña, J.L.G. Fierro, S. Rojas, *Int. J. Hydrog. Energy.*, **2014**, *10*, 5309-5318. [Crossref], [Google Scholar], [Publisher]
[59]. Y. Zhu, B. Zhang, Z. Feng, D. Sheng Su, *Catal. Today*, **2016**, *260*, 112-118. [Crossref], [Google Scholar], [Publisher]
[60]. S. Li, Y. Hu, Q. Xu, J. Sun, B. Hou, Y. Zhang, *J. Power Sources*, **2012**, *213*, 265-269. [Crossref], [Google Scholar], [Publisher]
[61]. M. Sun, H. Liu, Y. Liu, J. Qu, J. Li, *Nanoscale.*, **2015**, *7*, 1250-1269. [Crossref], [Google Scholar], [Publisher]
[62]. Y. Gorlin, C. Chung, D. Nordlund, B. Clemens, T. Jaramillo, *Acs Catal.*, **2012**, *2*, 2687-2694. [Crossref], [Google Scholar], [Publisher]
[63]. S. Jiang, C. Zhu, S. Dong, *J. Mater. Chem.*, **2013**, *1*, 3593-3599. [Crossref], [Google Scholar], [Publisher]
[64]. Y. Gorlin, T. Jaramillo, *J. Am. Chem. Soc.*, **2010**, *132*, 13612-13614. [Crossref], [Google Scholar], [Publisher]
[65]. C. Goswami, K.K. Hazarika, P. Bharali, *Mater. Sci. Technol.*, **2018**, *1*, 117-128. [Crossref], [Google Scholar], [Publisher]
[66]. R.F. Savinell, *Nat. chem.*, **2011**, *3*, 501-502. [Crossref], [Google Scholar], [Publisher]
[67]. J.B. Goodenough, B.L. Cushing, Handbook of Fuel Cells, **2010**. [Crossref], [Google Scholar], [Publisher]
[68]. M. Retuerto, F.C. Vallejo, L. Pascual, G. Lumbeeck, M. Fernandez-Diaz, M. Croft, J. Gopalakrishnan, *ACS Appl. Mater. Interfaces.*, **2019**, *11*, 21454-21464. [Crossref], [Google Scholar], [Publisher]
[69]. O. Hong, H. Lu, J. Wang, *ACS Sustain. Chem. Eng.*, **2017**, *5*, 9169-9175. [Crossref], [Google Scholar], [Publisher]
[70]. R. Zhou, Y. Zheng, D. Jurcakova, S. Qiao, *J. Mater. Chem.*, **2013**, *1*, 13179-13185. [Crossref], [Google Scholar], [Publisher]
[71]. Y. Liang, H. Wang, P. Diao, W. Chang, G. Hong, Y. Li, M. Gong, *J. Am. Chem. Soc.*, **2012**, *134*, 15849-15857. [Crossref], [Google Scholar], [Publisher]
[72]. B. Zhao, Y. Zheng, F. Ye, X. Deng, X. Xu, M. Liu, Z. Shao, *ACS Appl. Mater. Interfaces.*, **2015**, *7*, 14446-14455. [Crossref], [Google Scholar], [Publisher]
[73]. K. Huang, Y. Sun, Y. Zhang, X. Wang, W. Zhang, S. Feng, *Adv. Mater.*, **2019**, *31*, 1801430. [Crossref], [Google Scholar], [Publisher]
[74]. J. Huang, N. Zhu, T. Yang, T. Zhang, P. Wu, Z. Dang, *Biosens. Bioelectron*., **2015**, *72*, 332-339. [Crossref], [Google Scholar], [Publisher]
[75]. N. Andersen, A. Serov, P. Atanassov, *Appl. Catal. B.*, **2015**, *163*, 623-627. [Crossref], [Google Scholar], [Publisher]
[76]. N. Cheng, R. Kutz, C. Kemna, A. Wieckowski, *J. Electroanal. Chem.*, **2013**, *705*, 8-12. [Crossref], [Google Scholar], [Publisher]
[77]. M. Gao, J. Jiang, S. Yu, *Small*, **2012**, *8*, 13-27. [Crossref], [Google Scholar], [Publisher]
[78]. K. Lee, L. Zhang, J. Zhang, *Electrochem. commun*., **2007**, *9*, 1704-1708. [Crossref], [Google Scholar], [Publisher]
[79]. M.A Abdelkareem, T. Wilberforce, K. Elsaid, E. Sayed, E. Abdelghani, G. Olabi, *Int. J. Hydrog. Energy.*, **2021**, *46*, 23529-23547. [Crossref], [Google Scholar], [Publisher]
[80]. Y. Dong, Y. Deng, J. Zeng, H. Song, S. Liao, *J. Mater. Chem.*, **2017**, *5*, 5829-5837. [Crossref], [Google Scholar], [Publisher]
[81]. X.F. Lu, B. Xia, S. Zang, X. Lou, *Angew. Chem.*, **2020**, *132*, 4662-4678. [Crossref], [Google Scholar], [Publisher]
[82]. L. Sun, M.G. Campbell, M. Dincă, *Angew. Chem. Int. Ed.*, **2016**, *55*, 3566-3579. [Crossref], [Google Scholar], [Publisher]

[83]. S. Dang, Q. Zhu, Q. Xu, *Nat. Rev. Mater.*, **2017**, 3, 1-14. [Crossref], [Google Scholar], [Publisher]
[84]. S. Jin, *ACS Energy Lett.*, **2019**, *4*, 1443-1445. [Crossref], [Google Scholar], [Publisher]
[85]. P.Q. Liao, J.Q. Shen, J.P. Zhang, *Coord. Chem. Rev.,* **2018**, *373*, 22-48. [Crossref], [Google Scholar], [Publisher]
[86]. S. Agarwal, X. Yu, A. Manthiram, *Mater. Today Energy.*, **2020**, *16*, 100405. [Crossref], [Google Scholar], [Publisher]
[87]. J. Tan, X. He, F. Yin, B. Chen, X. Liang, G. Li, H. Yin, *Int. J. Hydrog. Energy*, **2020**, *45*, 15453-15464. [Crossref], [Google Scholar], [Publisher]
[88]. K. Huang, C. Rong, W. Zhang, X. Yang, Y. Fan, L. Liu, Z. Yang, W. Chen, J. Yang, *Mater. Today Energy*, **2021**, *19*, 100579. [Crossref], [Google Scholar], [Publisher]
[89]. N. Wang, Y. Li, Z. Guo, H. Li, S. Hayase, T. Ma, *J. Electrochem. Soc.*, **2018**, *165*, G3080. [Crossref], [Google Scholar], [Publisher]
[90]. Strelko V.V., Kuts V.S., Thrower P.A., *Carbon New York. NY.*, **2000**, *38*, 1499-1503. [Crossref], [Google Scholar], [Publisher]
[91]. E. Cruz-Silva, F. Urias, E. Sandoval, B. G. Sumpter, H. Terrones, J. Charlier, V. Meunier, M. Terrones, *Nanoscale*, **2011**, *3*, 1008-1013. [Crossref], [Google Scholar], [Publisher]
[92]. K.P. Singh, E.J. Bae, J.S. Yu, *J. Am. Chem. Soc.*, **2015**, *137*, 3165-3168. [Crossref], [Google Scholar], [Publisher]
[93]. F. Razmjooei, K.P. Singh, E.J. Bae, J.S. Yu, *J. Mater. Chem.*, **2015**, *3*, 11031-11039. [Crossref], [Google Scholar], [Publisher]
[94]. Z. Dong,G. Liu, S. Zhou, Y. Zhang, W. Zhang, A. Fan, X. Zhang, X. Dai, *Chem. Cat. Chem*., **2018**, *10*, 5475-5486. [Crossref], [Google Scholar], [Publisher]
[95]. Z.F. Wu, B. Tan, W. Ma, W. Xiong, Z.L. Xie, X.L. Huang, *Dalton Trans.*, **2018**, *47*, 2810-2819. [Crossref], [Google Scholar], [Publisher]
[96]. Y. Jing, Y. Cheng, L. Wang, Y. Liu, B. Yu, C. Yang, *Chem. Eng.*, **2020**, *397*, 125539. [Crossref], [Google Scholar], [Publisher]
[97]. L. Wan, E. Shamsaei, C. Easton, D. Yu, Y. Liang, X. Chen, Z. Abbasi, A. Akbari, X. Zhang, H. Wang, *Carbon*, **2017**, *121*, 330-336. [Crossref], [Google Scholar], [Publisher]
[98]. L. Chai, L. Zhang, X. Wang, L. Xu, C. Han, T. Li, Y. Hu, J. Qian, S. Huang, *Carbon*, **2019**, *146*, 248-256. [Crossref], [Google Scholar], [Publisher]
[99]. M. Zhang, D. Wu, Y. Ye, L. Wu, Z. Yao, X. Ma, L. Wang, Z. Zhang, S. Xiang, *Chem. Plus. Chem*., **2018**, *83*, 1044-1051. [Crossref], [Google Scholar], [Publisher]
[100]. A. Swami, I. Patil, M. Lokanathan, S. Ingavale, B. Kakade, *Chemistry Select*., **2020**, *5*, 3486-3493. [Crossref], [Google Scholar], [Publisher]
[101]. S. Shrestha, Y. Liu, W.E. Mustain, *Catal. Rev.*, **2011**, *53*, 256-336. [Crossref], [Google Scholar], [Publisher]
[102]. L. Zhang, L. Li, H. Chen, Z. Wei, *Chem Eur.*, **2019**, 26, 3973-3990. [Crossref], [Google Scholar], [Publisher]
[103]. C. Hu, L. Dai, *Angew. Chem. Int. Ed.*, **2016**, *55*, 11736-11758. [Crossref], [Google Scholar], [Publisher]
[104]. X. Liu, L. Dai, *Nat. Rev. Mater.*, **2016**, *1*, 1-12. [Crossref], [Google Scholar], [Publisher]
[105]. C. Hu, L. Dai, *Adv. Mater.*, **2017**, *29*, 1604942. [Crossref], [Google Scholar], [Publisher]
[106]. F. Zhang, J. Miao, W. Liu, D. Xu, X. Li, *Int. J. Hydrog. Energy.*, **2019**, *44*, 30986-30998. [Crossref], [Google Scholar], [Publisher]
[107]. T. Pan, H. Y. Liu, G. Ren, Y. Li, X. Lu, Y. Zhu, *Sci. Bull.*, **2016**, 66, 889-896. [Crossref], [Google Scholar], [Publisher]
[108]. L. Feng, Y. Yan, Y. Chen, L. Wang, *Energy Environ. Sci.*, **2011**, *4*, 1892-1899. [Crossref], [Google Scholar], [Publisher]
[109]. C.V. Rao, Y. Ishikawa, *J. Phys. Chem. C.*, **2012**, *116*, 4340-4346. [Crossref], [Google Scholar], [Publisher]
[110]. C. He, J.J, Zhang, P.K. Shen, *J. Mater. Chem*., **2014**, *2*, 3231-3236. [Crossref], [Google Scholar], [Publisher]
[111]. B. Guo, R. Ma, Z. Li, S. Guo, J. Luo, M. Yang, Q. Liu, T. Thomas, J. Wang, *Micro Nano Lett.*, **2020**, *12*, 1-13. [Crossref], [Google Scholar], [Publisher]
[112]. J. Lian, J. Zhao, X. Wang, *Acta Metallurgica Sinica.*, **2021**, *34*, 1-15. [Crossref], [Google Scholar], [Publisher]
[113]. F. Peng, H.J. Wang, H. Yu, W. Zheng, J. Yang, *Angew. Chem. Int. Ed.*, **2011**, *50*, 3257-3261. [Crossref], [Google Scholar], [Publisher]
[114]. R. Li, Z. Wei, X. Gou, W. Xu, *RSC Adv.*, **2013**, *3*, 9978-9984. [Crossref], [Google Scholar], [Publisher]

[115].
[116]. N. Daems, X. Sheng, F.J. Vankelecom, P.P. Pescarmona, *J. Mater. Chem.*, **2014**, *2*, 4085-4110. [Crossref], [Google Scholar], [Publisher]
[117]. L. Jiang, L. Sheng, Z. Fan, *Sci. China Mater.*, **2018**, *61*, 133-158. [Crossref], [Google Scholar], [Publisher]
[118]. C. Zhang, R. Hao, H. Liao, Y. Hou, *Nano Energy*, **2013**, *2*, 88-97. [Crossref], [Google Scholar], [Publisher]
[119]. Y. Zhan, J. Huang, Z. Lin, X. Yu, D. Zeng, X. Zhang, F. Xie, W. Zhang, J. Chen, H. Meng, *Carbon*, **2015**, *95*, 930-939. [Crossref], [Google Scholar], [Publisher]
[120]. G.A. Ferrero, Guillermo, A.B. Fuertes, M. Sevilla, M.M. Titirici, *Carbon*, **2016**, *106*, 179-187. [Crossref], [Google Scholar], [Publisher]
[121]. M. Zhou, H. Wang, S. Guo, *Chem. Soc. Rev.*, **2016**, *45*, 1273-1307. [Crossref], [Google Scholar], [Publisher]
[122]. D.W. Wang, F. Li, Z.G. Chen, G.Q. Lu, H.M. Cheng, *Chem. Mater.*, **2008**, *20*, 7195-7200. [Crossref], [Google Scholar], [Publisher]
[123]. J. Wu, L. Xiong, B. Zhao, M. Liu, and L. Huang, *Small Methods.*, **2020**, *4*, 1900540. [Crossref], [Google Scholar], [Publisher]
[124]. L. Cui, L. Cui, Z. Li, J. Zhang, H. Wang, S. Lu, Y. Xiang, *J. Mater. Chem.*, **2019**, *7*, 16690-16695. [Crossref], [Google Scholar], [Publisher]
[125]. M. Xiao, J. Zhu, G. Li, N. Li, S. Li, Z. Cano, L. Ma, *Angew. Chem. Int. Ed.*, **2019**, *58*, 9640-9645. [Crossref], [Google Scholar], [Publisher]
[126]. D. Wang, C. Ao, X. Liu, S. Fang, Y. Lin, W. Liu, W. Zhang, X. Zheng, L. Zhang, T. Yao, *ACS Appl. Energy Mater.*, **2019**, *2*, 6497-6504. [Crossref], [Google Scholar], [Publisher]
[127]. F. Li, G. Han, H. Noh, S. Kim, Y. Lu, H. Jeong, Z. Fu, J. Baek, *Energy Environ. Sci.*, **2018**, *11*, 2263-2269. [Crossref], [Google Scholar], [Publisher]
[128]. G. Wan, P. Yu, H. Chen, J. Wen, C. Sun, H. Zhou, N. Zhang, *Small*, **2018**, *14*, 1704319. [Crossref], [Google Scholar], [Publisher]
[129]. X. Ao, W. Zhang, Z. Li, J. Li, L. Soule, X. Huang, W. Chiang, *ACS nano*, **2019**, *13*, 11853-11862. [Crossref], [Google Scholar], [Publisher]
[130]. M. Xiao, L. Gao, Y. Wang, X. Wang, J. Zhu, Z. Jin, C. Liu, *J. Am. Chem. Soc.*, **2019**, *141*, 19800-19806. [Crossref], [Google Scholar], [Publisher]
[131]. E. Luo, H. Zhang, X. Wang, L. Gao, L. Gong, T. Zhao, Z. Jin, *Angew. Chem.*, **2019**, *131*, 12599-12605. [Crossref], [Google Scholar], [Publisher]
[132]. M. Xiao, J. Zhu, L. Ma, Z. Jin, J. Ge, X. Deng, Y. Hou, *ACS Catal.*, **2018**, *8*, 2824-2832. [Crossref], [Google Scholar], [Publisher]
[133]. L. Yang, D. Cheng, H. Xu, X. Zeng, X. Wan, J. Shui, Z. Xiang, D. Cao, *Proc. Natl. Acad. Sci. U. S. A.*, **2018**, *115*, 6626-6631. [Crossref], [Google Scholar], [Publisher]

Fawad Ahmad: He received his Ph.D. degree in physical chemistry in 2018 from University of Science and Technology of China (USTC) under the supervision of Professor Jie Zeng Group at Hefei National Laboratory for Physical Sciences at Microscale USTC. He moved back to his homeland and join University of Wah, Wah-Cantt, Pakistan as assistant professor of chemistry in august 2019. His work is focused on synthesis of nanomaterials and its catalytic application for fuel cell and water decontamination.

Khushboo-e-Kainat: She earned her BS degree in chemistry from university of wah in 2018. Currently she is pursuing MS in inorganic chemistry from the same university under the supervision of Dr. Fawad Ahmad, her research interest is synthesis of novel catalyst having high ORR activity.

Umar Farooq: He received his PhD from USTC and currently serving in the education university Lahore. His research interest is synthesis of energy material its functionalization and its electrochemical application.